

Exploration of new 212 MAB phases: M_2AB_2 (M=Mo, Ta; A=Ga, Ge) via DFT calculations

A. K. M Naim Ishtiaq^{1,2#}, Md Nasir Uddin^{1,2#}, Md. Rasel Rana^{1,2}, Shariful Islam^{1,2}, Noor Afsary¹, Karimul Hoque^{1,*}, Md. Ashraf Ali^{2,†}

¹ Physics Discipline, Khulna University, Khulna 9208, Bangladesh.

²Advanced Computational Materials Research Laboratory (ACMRL), Department of Physics, Chittagong University of Engineering and Technology (CUET), Chattogram-4349, Bangladesh.

*hoquekarimul@phy.ku.ac.bd, †ashrafphy31@cuet.ac.bd

Abstract

The recently developed MAB phases, an extension of the MAX phase, have sparked interest in research among scientists because of their better thermo-mechanical properties. In this paper, we have explored four new MAB phases M_2AB_2 (M=Mo, Ta and A=Ga, Ge) and studied the elastic, electronic, thermal, and optical properties to predict the possible applications. The stability of the new phases has been confirmed by calculating formation energy (E_f), formation enthalpy (ΔH), phonon dispersion curve (PDC), and elastic constant (C_{ij}). The study reveals that M_2AB_2 (M=Mo, Ta and A=Ga, Ge) exhibit significantly higher elastic constants, elastic moduli, and Vickers hardness values than their counterpart 211 borides. Higher Vickers hardness values of Ta_2AB_2 (A=Ga, Ge) than Mo_2AB_2 (A=Ga, Ge) have been explained based on the values of the bond overlap population. The analysis of the density of states and electronic band structure revealed the metallic nature of the borides under examination. The thermodynamic characteristics of M_2AB_2 (M=Mo, Ta and A=Ga, Ge) under high temperatures (0–1000 K) are investigated using the quasi-harmonic Debye model. Critical thermal properties such as melting temperature (T_m), Grüneisen parameter (γ), minimum thermal conductivity (K_{min}), Debye temperature (Θ_D), and others are also computed. Compared with 211 MAX phases, the 212 phases exhibit higher values of (Θ_D) and T_m , along with a lower value of K_{min} . These findings suggest that the studied compounds exhibit superior thermal properties that are suitable for practical applications. The optical characteristics have been examined, and the reflectance spectrum indicates that the materials have the potential to mitigate solar heating across various energy regions.

[#]First two authors contributed equally.

Keywords: 212 MAB phases; DFT; Structural properties; Mechanical properties; Thermal properties; Optical properties.

1. Introduction

The MAX phase has garnered significant attention in the present era due to its outstanding mechanical and thermal characteristics at high temperatures, showcasing attributes shared by both metals and ceramics. The increased interest in MAX phase materials can be traced back to Barsoum's noteworthy contributions [1], [2]. The term MAX phase represents a family of multilayer solids where M is an earlier transition metal, A is an element from the IIIA or IVA group of the periodic table, and X is an atom of C/N/B [3]. MAX phase materials showcase metallic behavior due to alternate metallic A-layers and ceramic behavior attributed to the MX layers [4]. Like most metals and alloys, MAX phase materials have excellent thermal shock resistance, superior machinability, and enhanced thermal and electrical conductivities. On the other hand, they have high melting or decomposition temperatures and strong elastic stiffness, similar to many ceramics[5]. The unique combination of metallic and ceramic properties makes them versatile, with applications ranging from high-temperature coatings to nuclear accident-tolerant fuel (ATF), concentrated solar power (CSP), catalysis, and as precursors for MXenes [6], [7], [8], [9].

The diversity of MAX phases was confined to C and N as X elements for years (from 1960 to 2014). However, recent advancements have overcome this limitation by successfully synthesizing MAX phases that contain B [10]. The physical and chemical properties of B and B-containing compounds highlight the potential of MAX phase borides, which replace C/N with boron [11]. Due to the presence of B in the composition, they are also called the MAB phase. Furthermore, scientific communities are actively working to broaden the diversity of MAX phases by introducing structural changes, as seen in examples like Cr_3AlB_4 (space group *Immm*), Cr_4AlB_6 (space group *Cmmm*), Cr_4AlB_4 [12], [13], [14]. Khazaei *et al.* reported on the first investigation of the theoretical MAX phase borides M_2AlB (where M = Sc, Ti, Cr, Zr, Nb, Mo, Hf, or Ta). They evaluated these compounds' electronic structure, mechanical characteristics, and dynamical stability in their investigation [15]. The diversity of MAX phases is a subject of research interest due to their structure variations and the number of atoms in the compounds, resulting in changes to their characteristics. In examples like the 211 MAX phase [16], 312 MAX

phase [8][17], 212 MAX phase [3], and i-MAX phase [18], the recent additions to the MAX family include the 314 MAX phase and 212 MAX phase, where the element B has been incorporated as an X element [3] [19]. This introduces a novel aspect to the MAX phase family, contributing to its diversity. The unique structural features of MAB phases include both orthorhombic and hexagonal symmetry observed in crystals. These distinctive symmetries set MAB phases apart from the typical MAX phases. Yinqiao Liu's synthesis of the orthorhombic phase of M_2AlB_2 , particularly the 212-MAB phases with $M = Sc, Ti, Zr, Hf, V, Nb, Cr, Mo, W, Mn, Tc, Fe, Co,$ and Ni , has revealed unique structural stability and notable electrical and mechanical properties [20]. The MAB phase structure slightly differs from the standard MAX phases, which typically crystallize in the hexagonal system with a space group $P-6m_2$ (No. 187). Ali *et al* [3]. investigated the diverse physical properties of Zr_2AB_2 ($A = In, Tl$). Martin Ade *et al* [13] synthesized ternary borides, namely Cr_2AlB_2 , Cr_3AlB_4 , and Cr_4AlB_6 , and subsequently compared their mechanical properties. Qureshi *et al.* [19] investigated the 314 Zr_3CdB_4 MAX phase boride, calculating its mechanical, thermodynamic, and optical properties. The 314 MAX phase Hf_3PB_4 has been thoroughly studied using Density Functional Theory (DFT) and revealed that it was the hardest MAX phase compound discovered until that date [21].

The structure of 212 phases exhibits a slight deviation from 211 MAX phases. In the case of 212 phases, a 2D layer of B is situated between M layers, featuring an additional B atom at the X position, unlike in 211 phases [22] [23], [24]. The B-B bonding in 212 MAX phase borides has improved mechanical and thermal properties. To date, the physical properties of Zr_2AB_2 ($A = In, Tl$) [25] and Hf_2AB_2 ($A = In, Sn$) [26], M_2AB ($M = Ti, Zr, Hf; A = Al, Ga, In$) [27] MAX phases, as well as Nb_2AC ($A = Ga, Ge, Tl, Zn, P, In,$ and Cd) MAX phases, have been investigated using density functional theory (DFT). In each instance, the mechanical properties of B-containing compounds show significant improvement compared to their traditional C/N containing 211 MAX phases.

The Debye temperature and melting temperature are higher for boron-containing 212 phases than for 211 carbides/nitrides, while the minimum thermal conductivity is lower. The thermal expansion coefficient of borides remains well-suited for use as coating materials. Consequently, the superior thermomechanical properties of B-containing 212 MAX phases demonstrate their suitability for high-temperature technological applications, surpassing the commonly used 211 MAX phase carbides. It should be noted that the 212 MAB phase with a hexagonal structure has

already been synthesized [24]. In addition, Ga and Ge-based MAX phases have also been synthesized previously [28]. Thus, the reports on the synthesis of 212 phase and Ga and Ge-based MAX phases motivated us to select the 212 MAB phases: M_2AB_2 ($M = Mo, Ta$; $A = Ga, Ge$) for our present study, and we have performed an in-depth investigation of their physical properties through DFT method.

Therefore, in this paper, the first-time prediction of the stability and mechanical, electronic, thermal, and optical properties of M_2AB_2 ($M = Mo, Ta$; $A = Ga, Ge$) phases has been presented. The results revealed that M_2AB_2 ($M = Mo, Ta$; $A = Ga, Ge$) compounds are stable and suitable for thermal barrier coating (TBC) and reflection coating applications. Additionally, to provide a comparison, the properties determined for M_2AB_2 ($M = Mo, Ta$, and $A = Ga, Ge$) are compared with those of other 212 and 211 compounds MAX phase borides.

2. Methods of calculations

First principles density-functional theory (DFT) computations are conducted utilizing the Cambridge Serial Total Energy Package (CASTEP) module integrated within Materials Studio 2017 [29], [30]. The exchange-correlation function is estimated using the Generalized Gradient Approximation (GGA) method, originally suggested by Perdew, Burke, and Ernzerhof [31]. Pseudo-atomic simulations accounted for electronic orbitals corresponding to B ($2s^2 2p^1$), Ga ($3d^{10} 4s^2 4p^1$), Ge ($4s^2 4p^2$), Mo ($4s^2 4p^6 4d^5 5s^1$), and Ta ($5d^3 6s^2$). The energy cutoff and k -point grids were established at 650 eV and $11 \times 11 \times 4$, respectively. The structural relaxation was performed utilizing the Broyden-Fletcher-Goldfarb-Shanno (BFGS) technique [32], while the electronic structure was computed employing density mixing. The parameters for relaxed structures incorporate the following tolerance thresholds: the self-consistent convergence of the total energy is set at 5×10^{-6} eV/atom, the maximum force exerted on the atom is limited to 0.01 eV/Å, the maximum ionic displacement is constrained to 5×10^{-4} Å, and a maximum stress threshold of 0.02 GPa is imposed. The finite strain method [33], grounded in density functional theory (DFT), is utilized to compute the elastic properties within this framework. All necessary equations for determining various properties are provided in the supplementary document.

3 Results and discussion

3.1 Structural properties

The M_2AB_2 compounds (where $M=Mo$ or Ta ; $A=Ga$ or Ge) belong to the $P6m_2$ (No. 187)[23] space group and crystallize in the hexagonal system. Unlike conventional MAX phases, which typically belong to the $P6_3/mmc$ (194) space group, the 212 MAX phases exhibit distinct characteristics. In Fig. 1, the unit cell structure of Mo_2GaB_2 is depicted as a representative of M_2AB_2 alongside Mo_2GaB , facilitating a comparison to discern their differences easily. The atomic positions are as follows: M (Mo or Ta) at (0.3333, 0.6667, 0.6935), A at (0.6667, 0.3333, 0.0), and two B atoms positioned at (0.6667, 0.3333, 0.5) and (0.0, 0.0, 0.5). The B components are arranged at the corners of the unit cell in typical 211 MAX phases, but in 212 boride MAX phases, they form a 2D layer between the M layers. This structural arrangement results in B-B covalent bonds in the 2D layer, enhancing stability compared to conventional 211 MAX phases.

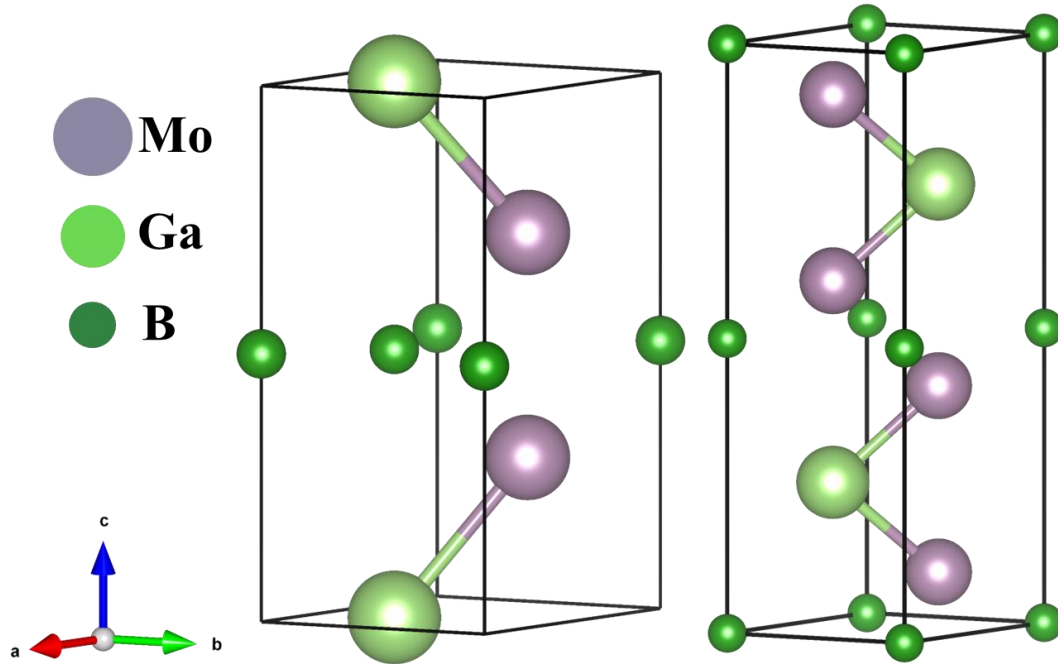


Fig. 1 - The schematic unit cell of (a) Mo_2GaB_2 and (b) Mo_2GaB compound.

The calculated lattice parameters of M_2AB_2 are presented in Table 1 alongside those of other 211 and 212 MAX phases for comparison, demonstrating consistency with prior results [16], [34], [35] and affirming the accuracy of the computational methodology used. The primary distinction between 212- and 211-unit cell structures arises from differences in the lattice parameter c ,

where the c value for 211 exceeds that of 212. Moreover, the volumes of Mo- and Ta-based 211 MAX phase borides surpass those of 212 MAX phase borides.

Table 1-Calculated lattice constants (*a* and *c*), *c/a* ratio, and volume (*V*) of M_2AB_2 .

Phase	Mo ₂ GaB ₂	Mo ₂ GeB ₂	Ta ₂ GaB ₂	Ta ₂ GeB ₂	^a Ti ₂ PB ₂	^b Mo ₂ GaB	^c Ta ₂ GaB
<i>a</i> (Å)	3.079	3.128	3.141	3.202	3.121	3.122	3.234
<i>c</i> (Å)	7.112	6.818	7.528	7.102	6.545	12.971	13.649
<i>c/a</i>	2.31	2.17	2.39	2.21	2.09	4.15	4.22
<i>V</i> (Å ³)	58.41	57.77	64.34	63.07	-	109	123.6

^aReference [34], ^bReference [16], ^cReference [35].

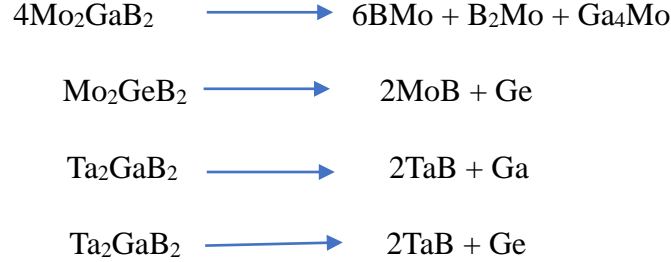
3.2 Stability

Examining a compound's stability is significant for multiple purposes, as it yields valuable information regarding the compound's synthesis parameters and aids in assessing the material's resilience across diverse environments, including thermal, compressive, and mechanical pressures. In this section, we delve into a comprehensive theoretical analysis concerning the chemical, dynamic, and mechanical stability of M_2AB_2 compounds.

The compound's chemical stability is determined by computing its formation energy by the following equation [36]: $E_{for}^{M_2AB_2} = \frac{E_{total}^{M_2AB_2} - (xE_{solid}^M + yE_{solid}^A + zE_{solid}^B)}{x+y+z}$. In the context provided, $E_{total}^{M_2AB_2}$ represents the total energy of the compound after optimizing the unit cell. E_{solid}^M , E_{solid}^A , and E_{solid}^B denote the energies of the individual elements M, A, and B, respectively. The variables *x*, *y*, and *z* correspond to the number of atoms in the unit cell for M, Ga, and B, respectively. For Mo₂GaB₂, Mo₂GeB₂, Ta₂GaB₂, and Ta₂GeB₂, the calculated formation energy (*E_f*) are -1.8079 eV/atom, -1.8859 eV/atom, -2.1252 eV/atom, and -2.1933 eV/atom, respectively. The negative values signify the chemical stability of all compounds. The order of chemical stability can be expressed as Ta₂GeB₂ > Ta₂GaB₂ > Mo₂GeB₂ > Mo₂GaB₂, indicating that Ta₂GeB₂ is the most stable. Additionally, it's observed that MAX phase borides containing Ta are more stable than those containing Mo.

Negative formation energy alone may not fully explain the chemical stability of M_2AB_2 (M=Mo, Ta and A=Ga, Ge). We calculated its formation enthalpy by examining potential pathways to evaluate its thermodynamic stability. For this analysis, we used the experimentally identified

stable phases of MoB[37] and TaB[38], Ga₄Mo[39], and B₂Mo[40]. The potential decomposition pathways for our compounds, as determined from the Open Quantum Materials Database (OQMD), are outlined below.



We have calculated the reaction energy as follows [41]:

$$E_{\text{reac}} = (\Delta H_f^{n\text{M}_2\text{AB}_2}) - \left(\sum_{\text{Stable phases}} \Delta H_f^{\text{products}} \right)$$

Where, M=Mo, Ta and A=Ga, Ge.

The following formula can calculate the decomposition energy associated with the reaction energy. $E_{\text{decom}} = \frac{E_{\text{reac}}}{n}$. Where n is the number of participating atoms. The calculated decomposition energies for Mo₂GaB₂, Mo₂GeB₂, Ta₂GaB₂, and Ta₂GeB₂ are -0.16, -0.17, -0.26, and -0.28 meV/atom, respectively. So, we can state that the M₂AB₂ (M=Mo, Ta and A=Ga, Ge) system exhibits thermodynamic stability.

Phonon dispersion curves (PDCs) have been calculated at the ground state utilizing the density functional perturbation theory (DFPT) linear-response approach to evaluate the dynamic stability of the MAX phase borides under investigation [42]. The PDCs, depicting the phonon dispersion along the high symmetry directions of the crystal Brillouin zone (BZ), along with the total phonon density of states (PHDOS) of M₂AB₂ (M=Mo, Ta; A=Ga, Ge) compounds, are illustrated in Fig. 2(a, b, c and d). Analysis of the PDCs reveals no negative phonon frequencies for any of the compounds, indicating their dynamic stability. The PHDOS of the M₂AB₂ compounds are derived from the PDCs and are presented alongside the PDCs in Fig. 2(a, b, c, and d), facilitating band identification through comparison of corresponding peaks. From Fig. 2, it is observed that in Mo₂GaB₂, the flatness of the bands for the Transverse Optical (TO) modes results in a prominent peak in the PHDOS, whereas non-flat bands for the Longitudinal Optical (LO) modes lead to weaker peaks in the PHDOS. Similar trends are observed in Mo₂GeB₂, Ta₂GaB₂, and

Ta₂GeB₂. Notably, a distinct discrepancy arises between the optical and acoustic branches, with the top of the LO and bottom of the TO modes situated at the *G* point, with separations of 7.49 THz, 6.39 THz, 9.39 THz, and 8.51 THz for Mo₂GaB₂, Mo₂GeB₂, Ta₂GaB₂, and Ta₂GeB₂ compounds, respectively.

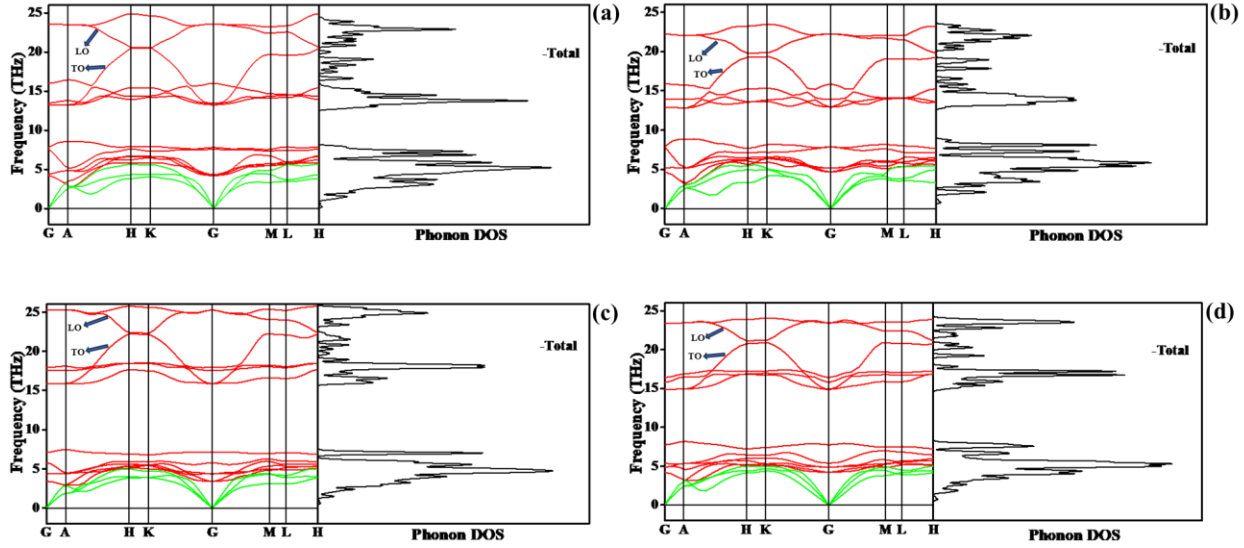


Fig. 2 – Phonon DOS and Phonon dispersion curves of (a) Mo₂GaB₂, (b) Mo₂GeB₂, (c) Ta₂GaB₂, and (d) Ta₂GeB₂ compounds.

Materials are subjected to various forces and loads in practical applications, necessitating understanding their mechanical stability. The mechanical stability of a compound can be assessed using stiffness constants. For a hexagonal system, the conditions for mechanical stability are as follows [43]: $C_{11} > 0$, $C_{11} > C_{12}$, $C_{44} > 0$, and $(C_{11} + C_{12})C_{33} - 2(C_{13})^2 > 0$. As indicated in Table 2, the C_{ij} values of M₂AB₂ (M=Mo, Ta; A=Ga, Ge) satisfy these conditions, thus confirming the mechanical stability of herein predicted phases: M₂AB₂ (M=Mo, Ta; A=Ga, Ge).

3.3 Electronic properties

Analyzing the electronic band structure (EBS) is crucial for gaining insights into the electronic behavior of a compound. The EBS of M₂AB₂ (M=Mo, Ta; A=Ga, Ge) MAX phases are depicted in Fig. 3(a, b, c, and d), with the Fermi energy (E_F) level set at 0 eV, represented by a horizontal line. Observing the EBS of M₂AB₂ (M=Mo, Ta; A=Ga, Ge), it is evident that the conduction band overlaps with the valence band, indicating the absence of a band gap. This observation confirms that the M₂AB₂ compounds exhibit metallic behavior, which aligns with conventional

MAX phases. The red lines illustrate the overlapping band at the Fermi level. Fig. 3 (a, b) shows that for Mo_2GaB_2 and Mo_2GeB_2 compounds, the maximum band overlap occurs along the A - H path. Conversely, in Fig. 3(c, d), the maximum band overlap is observed along the G - M paths. Utilizing the band structure, we can analyze the electrical anisotropy of M_2AB_2 MAX phase compounds. The anisotropic nature can be understood by analyzing the energy dispersion in the basal plane and along the c -axis. The paths G - A , H - K , and M - L show energy dispersion along the c -direction, and A - H , K - G , G - M , and L - H show energy dispersion in the basal plane. In comparison to the paths A - H , K - G , G - M , and L - H (basal plane), there is less energy dispersion along the lines G - A , H - K , and M - L (c -direction), as shown by Fig. 2(a, b, c and d). Lower energy dispersion in the c -direction results from a higher effective mass [44], indicating the strong electronic anisotropy of the M_2AB_2 MAX phase compound. Consequently, conductivity along the c -axis is expected to be lower than in the basal planes. These findings are consistent with prior studies [34], [45].

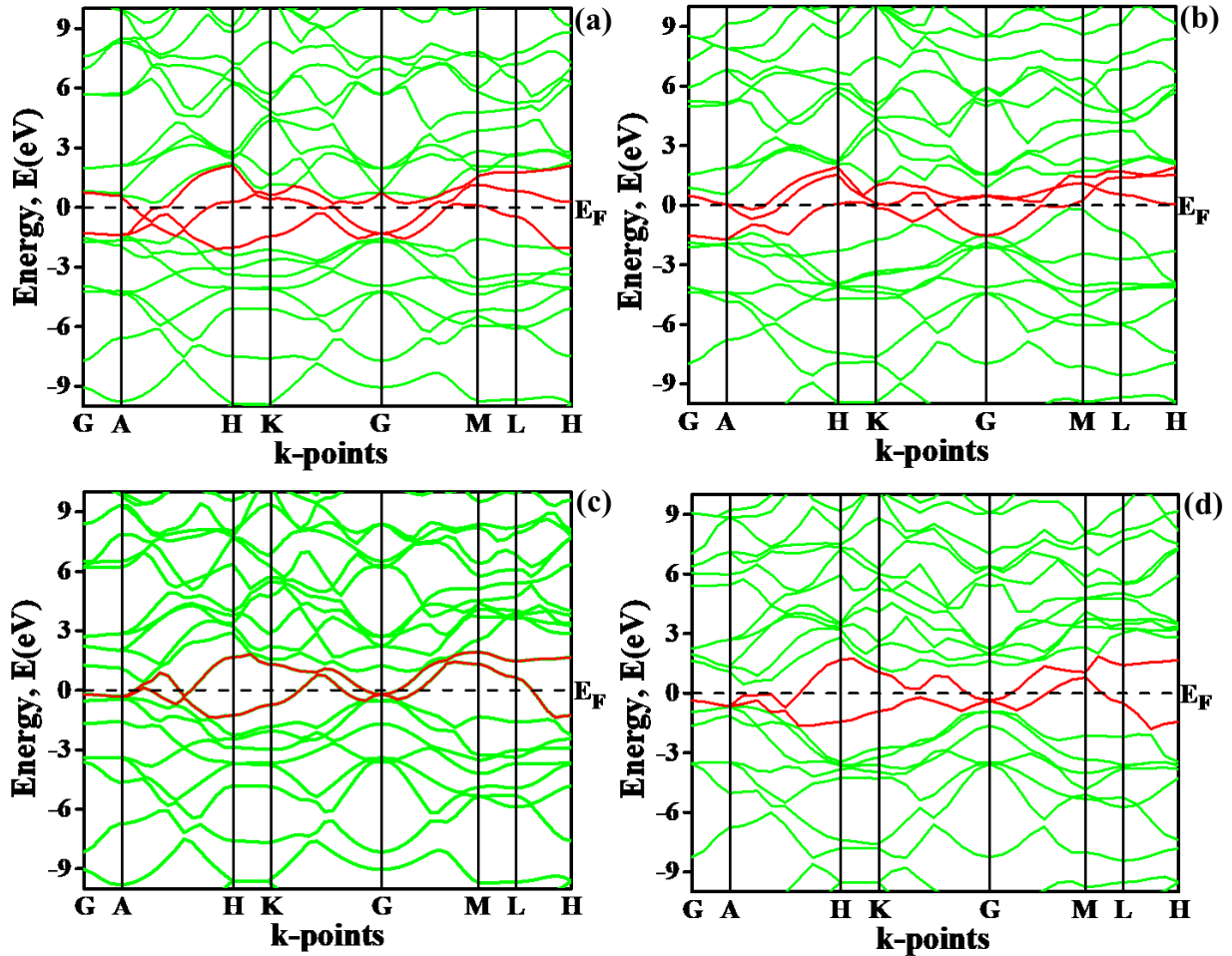


Fig. 3 – Band structure of (a) Mo_2GaB_2 , (b) Mo_2GeB_2 , (c) Ta_2GaB_2 , and (d) Ta_2GeB_2 compounds.

To investigate the bonding nature and electronic conductivity, the total density of states (TDOS) and partial density of states (PDOS) of M_2AB_2 compounds were computed. Figure 4 (a, b, c, and d) illustrates the TDOS and PDOS of these compounds, with the Fermi energy (E_F) set at zero energy level, indicated by a straight line. These profiles exhibit typical characteristics of MAX phase materials. The Mo or Ta-*d* electronic states predominantly contribute to the Fermi level, with a minor contribution from the B-*p* and Ga or Ge-*p* electronic states. To ascertain the hybridization characteristics of various electronic states within the valence band, the energy spectrum of the valence band has been partitioned into two distinct segments. The first segment encompasses the lower valence band region spanning from -7 eV to -3.5 eV, originating from the hybridization of Mo-*p*, Mo-*d*, and B-*s* orbitals in the case of the Mo_2GaB_2 compound. Conversely, for the Mo_2GeB_2 compound, the lower valence band region arises from the hybridization of Mo-*d*, Ge-*p*, and B-*s* orbitals. Notably, for both the Ta_2GaB_2 and Ta_2GeB_2 compounds, the dominance of the B-*p* state characterizes the lower valence band region. The second segment pertains to the upper valence band region from -3.5 eV to 0 eV. In the case of the Mo_2GaB_2 compound, this region arises from the hybridization of Mo-*p* and Mo-*d* orbitals. However, for the Mo_2GeB_2 , Ta_2GaB_2 , and Ta_2GeB_2 compounds, the upper valence band region results from the hybridization of Mo-*d* orbitals and (Ga/Ge)-*p* orbitals. Notably, the Fermi level of M_2AB_2 resides near the pseudogap in the TDOS profile, indicating a high level of electronic stability. Similar trends are observed in other compounds like Zr_2AlN , V_2AlN , Sc_2AlB , Sc_2GaB , Ta_2GaB , and Hf_2GaB_2 [15], [35], [45].

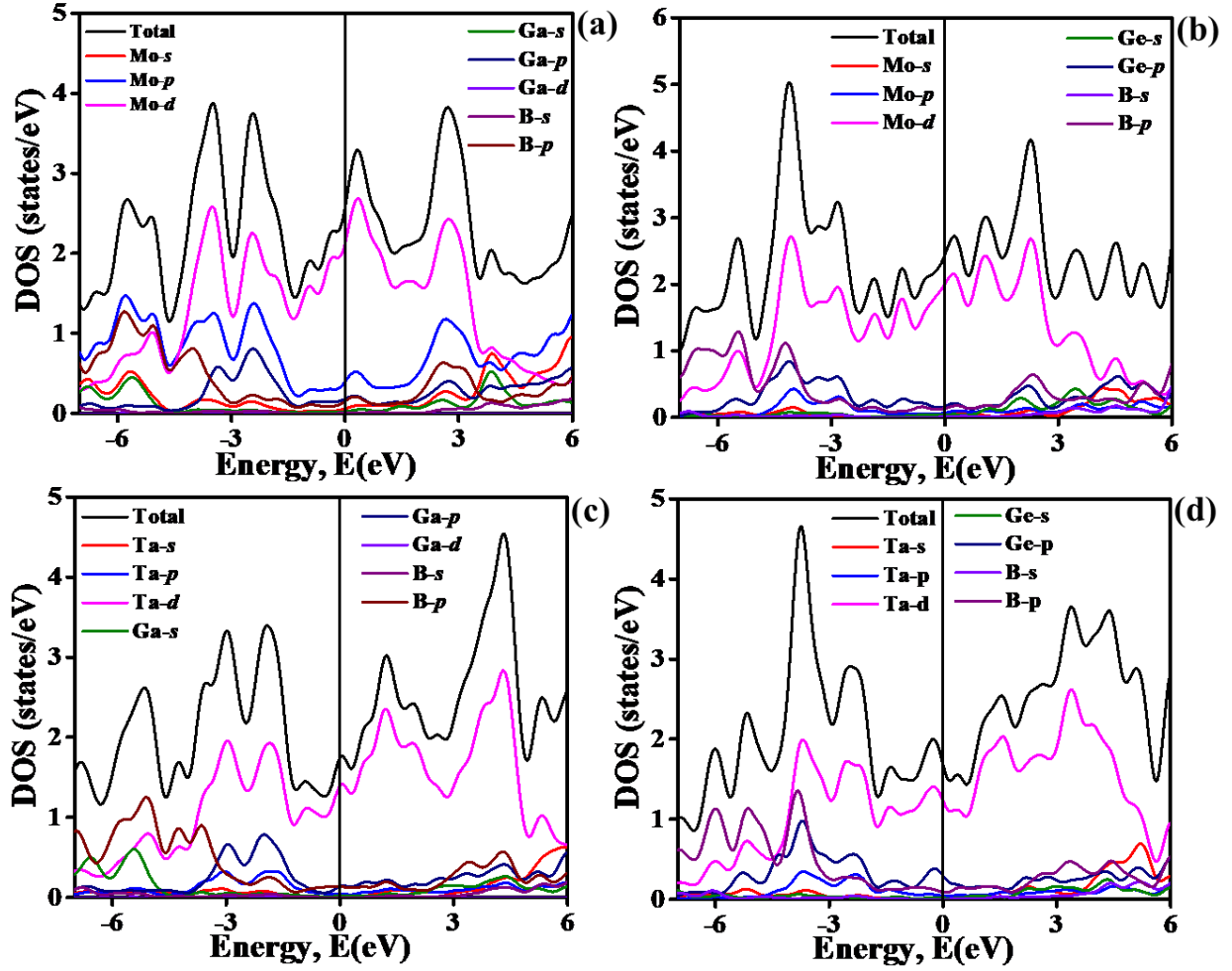


Fig. 4 – TDOS and PDOS of (a) Mo_2GaB_2 , (b) Mo_2GeB_2 , (c) Ta_2GaB_2 , and (d) Ta_2GeB_2 compounds.

The electron charge density mapping is helpful in understanding the distribution of electron densities linked to chemical bonds. It delineates areas of positive and negative charge densities, signifying the development and exhaustion of electrical charges, respectively. As depicted in the map, covalent bonds become apparent by accumulating charges between two atoms. Furthermore, the presence of ionic bonds can be inferred from a balance between negative and positive charges at specific atom positions[46]. The valence electronic CDM, denoted in units of $\text{e}\text{\AA}^{-3}$, for M_2AB_2 (where $\text{M} = \text{Mo}, \text{Ta}$; $\text{A} = \text{Ga}, \text{Ge}$) is showcased in Fig. 5(a, b, c, and d) along the (110) crystallographic plane. The accompanying scale illustrates the intensity of electronic charge density, with red and blue colors indicating low and high electronic charge density, respectively. As depicted in Fig. 5(a, b, c, and d), it is evident that charges accumulate in the regions between the B sites. Consequently, it is anticipated that strong covalent B–B bonding

occurs through the formation of two center-two electron ($2c-2e$) bonds in the M_2AB_2 (where $M=Mo, Ta$; $A=Ga, Ge$) compound, similar to other 212 MAX phase borides like Ti_2PB_2 , Zr_2PbB_2 , Nb_2SB_2 , Zr_2GaB_2 and Hf_2GaB_2 [34], [45]. Mulliken analysis has corroborated the charge transfer from Mo/Ta atoms to B atoms. The charge received from Mo/Ta atoms is distributed among the B atoms positioned at the transitions and those located at the edges, facilitating the formation of a two center-two electron ($2c-2e$) bond between B atoms within the 2D layer of B, as illustrated in Fig. 1(a). The hardness of each bond value presented in Table 5 also aligns with the results obtained from charge density mapping (CDM) and our analysis using moduli and elastic stiffness constants.

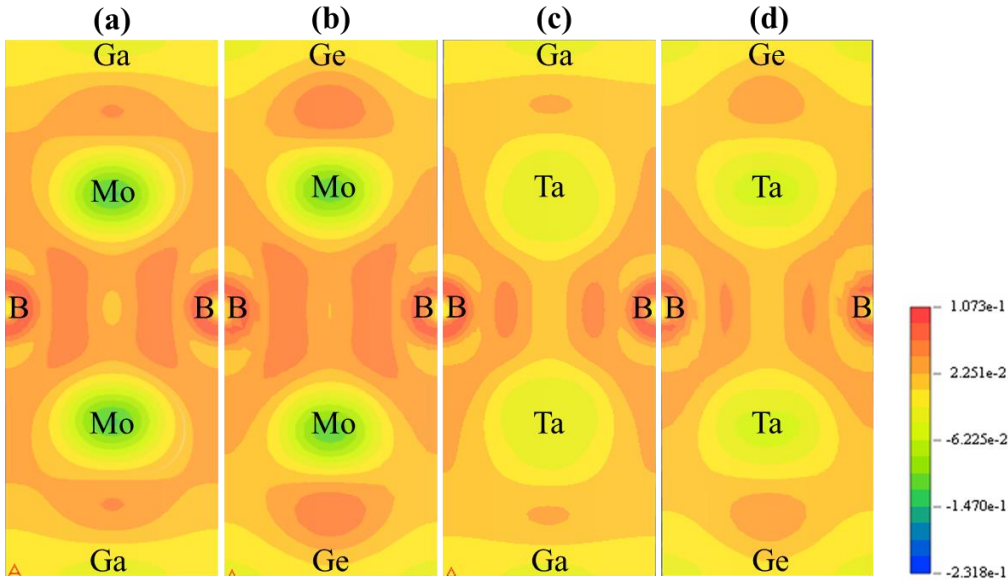


Fig. 5 – The charge density mapping of (a) Mo_2GaB_2 , (b) Mo_2GeB_2 , (c) Ta_2GaB_2 , and (d) Ta_2GeB_2 compounds.

3.4.1 Mechanical properties

The mechanical properties of materials play a pivotal role in determining their potential applications, serving as crucial indicators of their behavior and suitability in materials engineering endeavors. These properties are equally applicable to MAX phase materials. Initially, to assess the mechanical properties of the M_2AB_2 ($M=Mo, Ta$; $A=Ga, Ge$) phases, we employed the stress-strain method within the CASTEP code to compute the elastic constants (C_{ij}) [22], [47], [48]. These calculated elastic constants (C_{ij}) are presented in Table 2, alongside those

of other 212 and 211 MAX phases. Due to the hexagonal crystal structure of M_2AB_2 ($M=Mo, Ta$; $A=Ga, Ge$) phase borides, five stiffness constants emerge: C_{11} , C_{12} , C_{13} , C_{33} , and C_{44} [49]. The mechanical stability was evaluated using these stiffness constants in the preceding section. For instance, C_{11} and C_{33} determine stiffness when stress is exerted along the (100) and (001) directions, respectively, whereas C_{44} evaluates resistance to shear deformation on the (100) and (001) planes. The stiffness constants C_{11} and C_{12} directly reflect the strength of atomic bonds along the a - and c -axes. When C_{11} exceeds C_{33} (or vice versa), it signifies stronger atomic bonding along the a -axis (or c -axis). In Table 2, for Mo_2GaB_2 , Mo_2GeB_2 , and Ta_2GeB_2 compounds, C_{11} surpasses C_{33} , indicating superior atomic bonding along the a -axis compared to the c -axis. This robust bonding along the a -axis suggests heightened resistance to a -axial deformation. Conversely, in Ta_2GeB_2 , where $C_{11} < C_{33}$, stronger atomic bonding along the c -axis translates to increased resistance against c -axial deformation. Analysis of Table-2 reveals that the values of C_{11} and C_{22} are notably higher for 212 MAX phase borides than 211 MAX phase borides. Consequently, it can be inferred that 212 MAX phases exhibit stronger resistance to axial deformation when juxtaposed with 211 MAX phases. C_{44} is commonly utilized to gauge shear deformation tolerance among the elastic constants. Notably, Ta_2GaB exhibits superior shear deformation resistance owing to its highest C_{44} value among the studied compounds. Furthermore, the individual elastic constants C_{12} , C_{13} , and C_{44} denote shear deformation response under external stress. The observation that C_{11} and C_{33} possess larger magnitudes than C_{44} implies that shear deformation is more facile than axial strain. Another crucial parameter derived

Table 2- The stiffness constants, elastic moduli, Cauchy Pressure (CP), f -index, Pugh's ratio (G/B), fracture toughness (K_{IC}), and hardness parameters of M_2AB_2 .

Parameters	Mo_2GaB_2	Mo_2GeB_2	Ta_2GaB_2	Ta_2GeB_2	aTi_2PB_2	bTi_2InB_2	cZr_2TiB_2	dMo_2GaB	eTa_2GaB
C_{11} (GPa)	393	385	339	334	368	358	310	312	309
C_{33} (GPa)	322	372	332	395	383	270	251	246	278
C_{44} (GPa)	149	161	145	178	184	93	66	158	141
C_{12} (GPa)	125	164	128	186	90	52	52	95	107
C_{13} (GPa)	146	167	133	146	121	57	61	167	115
B_V (GPa)	216	238	199	224	-	-	-	192	174
B_R (GPa)	215	238	199	224	-	-	-	192	174
B (GPa)	215	238	199	224	198	145	135	192	174

G_V (GPa)	132	129	120	125	-	-	-	114	114
G_R (GPa)	129	124	117	107	-	-	-	87	109
G (GPa)	130	127	118	116	152	119	94	101	111
Y_V (GPa)	330	329	300	316	-	-	-	286	281
Y_R (GPa)	322	318	293	278	-	-	-	228	271
Y (GPa)	326	323	297	297	361	280	229	258	276
ν_V	0.245	0.269	0.249	0.265	-	-	-	0.252	0.232
ν_R	0.249	0.276	0.255	0.293	-	-	-	0.302	0.241
ν	0.247	0.273	0.252	0.279	0.19	-	0.22	0.276	0.236
CP	-36.10	2.66	-17.24	8.16	-94	-	-21	-	-33.96
G/B	0.60	0.53	0.59	0.51	0.77	0.821	.70	0.53	0.64
KIC ($MPa.m^{1/2}$)	2.53	2.62	2.36	2.47	-	-	-	2.16	2.21
f	1.284	1.045	1.010	0.918	-	-	-	0.937	1.142
H_{macro} (GPa)	16.32	13.35	14.76	11.98	24.74	-	15.7	11.051	15.75
H_{micro} (GPa)	22.04	19.23	19.61	17.14	30.79	-	17.7	15.098	19.68

^aReference [34], ^bReference [50], ^cReference [25], ^dReference [16], ^eReference [35].

from the stiffness constants is the Cauchy pressure (CP), calculated as $C_{12} - C_{44}$, which provides vital insights relevant to the practical applications of solids [51]. Pettifor [51] emphasized the significance of Cauchy pressure (CP) in discerning the chemical bonding and ductile/brittle properties of solids. A negative CP value indicates covalently bonded brittle solids, whereas a positive value signifies isotropic ionic ductile solids. Mo_2GaB_2 and Ta_2GaB_2 fall into covalently bonded brittle solids, while Mo_2GeB_2 and Ta_2GeB_2 exhibit metallic ductile characteristics. Similarly, like Ga-containing 211 MAX phase borides, Ga-containing 212 MAX phases also demonstrate negative CP values and brittle behavior [52][53].

The elastic constants obtained are used to produce several bulk elastic parameters that are used to characterize polycrystalline materials, such as Young's modulus (Y), bulk modulus (B), and shear modulus (G). In Table 2, the bulk modulus (B) and shear modulus (G) calculated using Hill's approximation [54] are also presented. Hill's values represent the average of the upper limit (Voigt [55]) and lower limit (Reuss [56]) of B . The necessary equations for these calculations are provided in the supplementary document (S1). Young's modulus (Y) is a crucial indicator of material stiffness. A higher Y value indicates a stiffer material. It can be observed from the table that Mo_2GaB_2 exhibits the highest Y value, signifying its greater stiffness compared to others.

According to the sequence of Y values, stiffness can be ranked as follows: $\text{Mo}_2\text{GaB}_2 > \text{Mo}_2\text{GeB}_2 > \text{Ta}_2\text{GaB}_2 > \text{Ta}_2\text{GeB}_2$. Therefore, Mo_2GaB_2 , with its higher Young's modulus, is anticipated to demonstrate superior mechanical stability and deformation resistance compared to the other compounds under investigation. This quality is essential for aircraft parts or high-performance machinery applications where critical dimensional stability and structural integrity are required [57], [58]. Table 2 shows that 212 MAX phase materials exhibit larger Young's modulus (Y) values than 211 MAX phases. This suggests that 212 MAX phase borides are stiffer than their 211 MAX phase counterparts. Young's modulus (E) also correlates well with thermal shock resistance (R): $R \propto 1/E$ [59]. Lower Young's modulus values correspond to higher thermal shock resistance. Therefore, materials with higher thermal shock resistance (i.e., lower Young's modulus) are more suitable for use as Thermal Barrier Coating (TBC) materials. Given that Ta_2GaB_2 possesses the lowest Y value among the materials studied, it should be considered a superior candidate for TBC material due to its higher thermal shock resistance. The material's ability to withstand shape distortion is elucidated by the shear modulus (G). On the other hand, the bulk modulus (B) indicates the strength of a material's chemical bonds and its ability to withstand uniform compression or volume change. We computed Young's modulus (Y), bulk modulus (B), and shear modulus for our analysis. Based on the bulk modulus values presented in Table 2, the sequence of a material that resists compression when pressure is applied can be outlined as follows: $\text{Mo}_2\text{GeB}_2 > \text{Ta}_2\text{GeB}_2 > \text{Mo}_2\text{GaB}_2 > \text{Ta}_2\text{GaB}_2$. Mo_2GeB_2 , boasting a higher bulk modulus, may exhibit reduced plastic deformation and superior resistance to stress-induced deformation compared to other compounds examined.

The ductile and brittle characteristics of the M_2AB_2 ($\text{M}=\text{Mo}, \text{Ta}$; $\text{A}=\text{Ga}, \text{Ge}$) compounds can also be assessed through Poisson's ratio (ν) and Pugh's ratio (G/B). A compound demonstrates ductile (brittle) behavior if the ν value surpasses (falls below) 0.26 [60]. Furthermore, if the G/B value exceeds (is less than) 0.571, then the compound exhibits brittle (ductile) behavior [19]. According to both criteria, Mo_2GaB_2 and Ta_2GaB_2 are classified as brittle compounds, whereas Mo_2GeB_2 and Ta_2GeB_2 are categorized as ductile compounds. The ductile nature of Ge-based MAX phases has been reported previously [61].

Fracture toughness (K_{IC}) is a vital property that gauges a material's ability to resist crack propagation. In the case of M_2AB_2 ($\text{M}=\text{Mo}, \text{Ta}$; $\text{A}=\text{Ga}, \text{Ge}$) compounds, Equation (S2) was

employed to determine K_{IC} . The K_{IC} values are documented in Table 2, and notably, these values surpass those of 211 MAX phases [16], [35]. Another parameter, the " f -index," characterizes the isotropic nature and strength of atom-atom bonds within a single hexagonal crystalline lattice along the a - and c -directions. If the f -index is less than 1, chemical bonds exhibit greater rigidity along the c -axis; conversely, if f exceeds 1, bonds are more rigid in the ab -plane. When the value of f is set to 1, atomic bonds exhibit similar strength and uniformity in all directions [15]. The f -value is computed using Equation (S3) and displayed in Table 2. Table 2 shows that the f -values of Mo_2GeB_2 , Ta_2GaB_2 , and Ta_2GeB_2 , which are close to one, indicate a slight anisotropic bonding strength. Nevertheless, substances with robust bonds in the horizontal plane (ab plane) ($f > 1$), such as Mo_2GaB_2 , are deemed optimal candidates for the exfoliation process. In engineering applications, the hardness of a solid material serves as a valuable criterion for designing various devices. The elastic properties of polycrystalline materials can be utilized to calculate hardness values, as the ability to resist indentation is closely linked to a material's hardness. Both micro-hardness (H_{micro}) and macro-hardness (H_{macro}) were computed using Equation (S4) and are presented in Table 2. Based on the values of H_{micro} and H_{macro} , Mo_2GaB_2 emerges as the toughest among the studied phases. The order of hardness is as follows: $\text{Mo}_2\text{GaB}_2 > \text{Ta}_2\text{GaB}_2 > \text{Mo}_2\text{GeB}_2 > \text{Ta}_2\text{GeB}_2$. Interestingly, Ga-containing MAX phase borides exhibit superior hardness compared to Ge-containing MAX phase borides. In Table 2, we compare our findings with previously reported MAX phases and observe that our data align perfectly with the earlier results.

3.4.2 Elastic anisotropy

Additionally, anisotropy is linked to other crucial events like anisotropic plastic deformation and the development and spread of micro-cracks within mechanical stress. By providing direction-dependent elastic constants, the understanding of anisotropy also offers a framework for improving the mechanical stability of materials in extreme circumstances. The following formulae are used for hexagonal structures to calculate the various anisotropic variables from elastic constants C_{ij} [62].

$$A_1 = \frac{\frac{1}{6}(C_{11}+C_{12}+2C_{33}-4C_{13})}{C_{44}}, A_2 = \frac{2C_{44}}{C_{11}-C_{12}} \text{ and } A_3 = A_1 \cdot A_2 = \frac{\frac{1}{3}(C_{11}+C_{12}+2C_{33}-4C_{13})}{C_{11}-C_{12}}$$

Table 3 lists every anisotropy parameter. Since the value of A_i should be 1 to be isotropic, the computed value of A_i ($i = 1-3$) indicates that all of the compounds under research exhibit anisotropic behavior [63].

Table 3: Data for Elastic anisotropy factors.

Phase	A_1	A_2	A_3	A_B	A_G	A^U
Mo₂GaB₂	0.65	1.12	0.73	0.22	1.35	0.14
Mo₂GeB₂	0.64	1.46	0.93	0.006	1.92	0.196
Ta₂GaB₂	0.69	1.38	0.95	0.0003	1.41	0.143
Ta₂GeB₂	0.68	2.4	1.63	0.02	7.56	0.818
^a Hf₂InB₂	1.16	0.67	0.78	-	-	0.177
^b Hf₂SnB₂	1.04	0.76	0.79	-	-	0.040
^c Zr₂PbB₂	1.22	0.63	0.77	-	-	0.45

^{a,b} Reference [64], ^c Reference [65].

An additional method for estimating elastic anisotropy is to use the percentage anisotropy to compressibility and shear (A_B & A_G). This gives polycrystalline materials a helpful way to measure elastic anisotropy. They have been described as [45];

$$A_B = \frac{B_V - B_R}{B_V + B_R} \times 100\% ; A_G = \frac{G_V - G_R}{G_V + G_R} \times 100\% \text{ and } A^U = 5 \frac{G_V}{G_R} + \frac{B_V}{B_R} - 6 \geq 0$$

Zero values for A_B , A_G , and the universal anisotropy factor (A^U) show elastic isotropy; the maximum amount of anisotropy is represented by a value of 1. Table 3 shows that, compared to other compounds, the values of A_B , A_G , and A^U for Mo₂GeB₂ and Ta₂GaB₂ are incredibly close to zero, suggesting that these compounds have nearly isotropic characteristics.

3.4.3 Mulliken Populations

The Mulliken charge assigned to an atomic species quantifies the effective valence by calculating the absolute difference between the formal ionic charge and the Mulliken charge. Equations (S5) and (S6) are employed to ascertain the Mulliken charge for each atom (α). Table-4 provides the Mulliken atomic population and effective valence charge. Transition metals Mo and Ta in M₂AB₂ (M = Mo, Ta, and A = Ga, Ge) have pure valence states of 4d⁵ and 5d³, respectively. The *d*-

orbital electrons of transition metals have been found to influence their effective valence charge significantly. A non-zero positive value indicates a combination of covalent and ionic attributes within chemical bonds. As this value decreases towards zero, it signifies a rise in ionicity. A zero value suggests an ideal ionic character in the bond. Conversely, a progression from zero with a positive value indicates an elevation in the covalency level of the bonds. Based on their effective valence, M atoms move from the left to the right in the periodic table, increasing the covalency of M_2AB_2 (M = Mo, Ta, and A = Ga, Ge). Table-4 reveals that the Mulliken atomic charge ascribed to the B atoms is solely negative. Conversely, positive Mulliken atomic charges are associated with transition metals (M) and A. This suggests a charge transfer from M and A to B for each compound within M_2AB_2 (where M = Mo, Ta, and A = Ga, Ge), thereby fostering ionic chemical bonds among these atoms. Bond population serves as another indicator of bond covalency within a crystal, as a high value of bond population essentially signifies a heightened degree of covalency within the chemical bond. The bonding and anti-bonding states influence the populations with positive and negative bond overlap. As demonstrated in Table-5, the B-B bond exhibits greater covalency compared to any other bond in M_2AB_2 (M = Mo, Ta, and A = Ga, Ge). The presence of an antibonding state between two relevant atoms, which subsequently decreases their chemical bonding, is indicated by a hostile bond overlap population. In Mo_2GeB_2 and Ta_2GeB_2 , a hostile bond overlap population is observed in the Ge-Mo and Ge-Ta bonds, indicating the presence of an antibonding state. Therefore, the existence of ionic bonding is guaranteed by electronic charge transfer. On the other hand, the high positive value of the bond overlap population (BOP) denotes the presence of covalent bonding, a feature shared by materials in the MAX phase.

Table 4-Data for Mulliken atomic populations and Effective valence charge of M_2AB_2 (M = Mo, Ta, and A = Ga, Ge) compounds.

Compound	Atom	Mulliken atomic population					Effective Vallance charge
		<i>s</i>	<i>p</i>	<i>d</i>	Total	Charge	
Mo₂GaB₂	B	0.89	2.57	0.00	3.46	-0.46	–
	B	0.90	2.58	0.00	3.48	-0.48	–
	Ga	0.69	1.84	9.99	12.52	0.48	2.52

	Mo	2.21	6.48	5.08	13.77	0.23	5.77
	Mo	2.21	6.48	5.08	13.77	0.23	5.77
Mo₂GeB₂	B	0.90	2.55	0.00	3.45	-0.45	–
	B	0.91	2.56	0.00	3.45	-0.47	–
	Ge	0.77	2.50	0.00	3.27	0.73	3.27
	Mo	2.28	6.50	5.12	13.91	0.09	5.91
	Mo	2.28	6.50	5.12	13.91	0.09	5.91
Ta₂GaB₂	B	1.01	2.58	0.00	3.59	-0.59	–
	B	1.02	2.60	0.00	3.62	-0.62	–
	Ga	0.32	1.90	9.99	12.21	0.79	2.21
	Ta	0.43	0.46	3.90	4.79	0.21	4.79
	Ta	0.43	0.46	3.90	4.79	0.21	4.79
Ta₂GeB₂	B	1.03	2.58	0.00	3.60	-0.60	–
	B	1.01	2.57	0.00	3.58	-0.58	–
	Ge	0.45	2.62	0.00	3.07	0.93	3.07
	Ta	0.43	0.47	3.98	4.87	0.13	4.87
	Ta	0.43	0.47	3.98	4.87	0.13	4.87

3.4.4 Theoretical Vickers Hardness

Vickers hardness, derived from the atomic bonds found in solids, indicates how resistant a material is to deformation in extreme circumstances. Several variables influence this feature, such as the crystal flaws, solid structure, atomic arrangement, and bond strength. The Vickers hardness of the M₂AB₂ (M = Mo, Ta, and A = Ga, Ge) MAX phases is determined using the Mulliken bond population method, as described by Gou et al. [66] using the formula (S7-S10). This method is particularly suitable for partial metallic systems such as MAX phases. Table-5 lists the computed Vickers hardness values for the M₂AB₂ (M = Mo, Ta, and A = Ga, Ge)

compounds. The calculated values are 3.35 GPa, 4.76 GPa, 8.21 GPa, and 8.74 GPa for Mo_2GaB_2 , Mo_2GeB_2 , Ta_2GaB_2 , and Ta_2GeB_2 , respectively. We observed that Ta_2GaB_2 and Ta_2GeB_2 have much higher hardness values than Mo_2GaB_2 and Mo_2GeB_2 . These values are also higher than that of other 212 phases, like, Ti_2InB_2 (4.05 GPa) [50], Hf_2InB_2 (3.94 GPa), and Hf_2SnB_2 (4.41 GPa) [26], Zr_2InB_2 (2.92 GPa) and Zr_2TlB_2 (2.19 GPa) [25], Zr_2GaB_2 (2.53GPa), Zr_2GeB_2 (3.31GPa), Hf_2GaB_2 (4.73GPa) and Hf_2GeB_2 (4.83GPa) [67]The H_v calculated by the geometrical average of the individual bonding, where the bonding strength mainly determined by the BOP values. In the case of Ta_2GaB_2 and Ta_2GeB_2 , the BOP of M-B bonding is much higher compared to Mo_2GaB_2 and Mo_2GeB_2 . Even though the BOP of M-B for Ta_2GaB_2 and Ta_2GeB_2 is higher than that of the other 212 phases mentioned earlier. Therefore, higher values of H_v are expected for Ta_2GaB_2 and Ta_2GeB_2 . Additionally, we looked at the Vickers hardness value between 211 and 212 compounds and discovered that the 212 MAX phase compounds had a higher H_v value. This is because a 2D layer of B atoms is positioned between the M atoms. The B atoms share two center-two electrons to form an extremely strong B-B bond [3].

Table 5 Calculated data for Mulliken bond number (n^μ), bond length (d^μ), bond overlap populations BOP, (P^μ), metallic populations ($P^{\mu'}$), Vickers hardness (H_v) M_2AB_2 (M = Mo, Ta, and A = Ga, Ge) compounds.

Compounds	Bond	n^μ	$d^\mu(\text{\AA})$	P^μ	$P^{\mu'}$	V_b^μ	H_v (Gpa)
Mo_2GaB_2	B1-B2	1	1.7779	2.15	0.016	5.89	
	B1-Mo1	2	2.3217	0.17	0.016	13.12	3.35
	B2-Mo2	2	2.3217	0.16	0.016	13.12	
Mo_2GeB_2	B1-B2	1	1.8059	2.15	0.031	5.96	
	B1-Mo1	2	2.3387	0.21	0.031	12.95	4.76
	B2-Mo2	2	2.3387	0.32	0.031	12.95	
	Ge1-Mo2	2	2.6381	-3.94	-	-	
Ta_2GaB_2	B1-B2	1	1.8136	2.08	0.008	6.18	
	B1-Ta1	2	2.4113	0.59	0.008	14.53	8.21
	B2-Ta2	2	2.4113	0.54	0.008	14.53	
Ta_2GeB_2	B1-B2	1	1.8488	2.08	0.008	6.22	8.74
	B1-Ta1	2	2.4345	0.63	0.008	14.21	
	B2-Ta2	2	2.4345	0.55	0.008	14.21	

	Ge1-Ta2	2	2.6997	-0.95	-	-	
^a Mo ₂ GaB	B-Mo	4	2.1641	1.10	0.004	27.37	3.25
^b Zr ₂ GeB ₂	B-B	1	1.8456	2.3	0.020	6.510	
	B-Zr	2	2.5072	0.19	0.020	16.31	2.53
	B-Zr	2	2.5072	0.16	0.020	16.31	
^c Ta ₂ GaB	B-Ta	4	2.2630	1.67	0.074	30.9	3.88

^aReference[16], ^bReference[45], ^cReference[35]

3.5 Thermal Properties

MAX phases are ideal for high-temperature applications due to their exceptional mechanical qualities at elevated temperatures. As a result, researching the fundamental parameters necessary for predicting their application is of great interest, and these can be obtained from the vibrations of atoms or phonons. The Debye temperature (Θ_D) of a solid is directly connected to its bonding strength, melting temperature, thermal expansion, and conductivity. Using the sound velocity and Anderson's technique [68], the Θ_D of the phases under study has been computed using the formula (S11). Equation (S12) can be used to get the average sound velocity (V_m) from the longitudinal and transverse sound velocities. Equations (S13–14) were used to determine v_l and v_t . The calculated values of Debye's temperature are shown in Table 6, where Mo₂GaB₂ has the highest Θ_D and Ta₂GeB₂ has the lowest. If we rank them, it is as follows: Mo₂GaB₂ < Mo₂GeB₂ < Ta₂GaB₂ < Ta₂GeB₂. Hadi et al. recently reported a MAX phase (V₂SnC) as a TBC material with a Θ_D value of 472 K [69]. Thus, M₂AB₂ (M = Mo, Ta, and A = Ga, Ge) exhibit encouraging potential as TBC materials, as shown in Table 6.

Table 6-Data for density (ρ), longitudinal, transverse, and average sound velocities (v_l , v_t , and v_m), Debye temperature (Θ_D), minimum thermal conductivity (K_{min}), Grüneisen parameter (γ), thermal expansion coefficient (TEC) at 300K and melting temperature (T_m) of M₂AB₂ (M = Mo, Ta, and A = Ga, Ge) compounds.

Phases	ρ (kg/m ³)	v_l (m/s)	v_t (m/s)	v_m (m/s)	Θ_D (K)	K_{min} (W/mK)	γ	TEC (K ⁻¹)	T_m (K)
Mo ₂ GaB ₂	8055	6959	4032	4475	585	1.20	1.49	1.52×10 ⁻⁶	2017
Mo ₂ GeB ₂	8227	7040	3932	4378	574	1.18	1.61	1.52×10 ⁻⁶	2069

Ta₂GaB₂	11702	5533	3185	3537	448	0.88	1.51	1.47×10 ⁻⁶	1870
Ta₂GeB₂	12013	5628	3112	3467	438	0.89	1.65	1.48×10 ⁻⁶	1950
^a Ti₂PB₂	4450	9480	5839	6442	861	1.71	1.26	-	2033
^b Mo₂GaB	8265	6291	3498	3896	480	0.940	1.63	-	1660
^c Ta₂GaB	11890	4004	999.8	1142	404.9	0.25	1.44		1700
^d Zr₂GaB₂	6334.81	6682	4050.28	4476.09	546	0.90	1.32		1684

^aReference[52], ^bReference[16], ^cReference[35], ^dReference [45]

The constant thermal conductivity value at high temperatures is the minimum thermal conductivity (K_{min}). As the name implies, this conductivity is minimal because, at high temperatures, phonon coupling breaks. The formula (S15) for the minimum thermal conductivity of solids was derived using the Clarke model [70]. Table 6 lists the calculated value of k_{min} , with Ta₂GaB₂ having the lowest value and Mo₂GaB₂ having the highest. When selecting suitable materials for TBC applications, a minimum thermal conductivity of 1.25 W/mK is used as a screening criterion [71]. Our compounds exhibit lower minimum thermal conductivity values, holding promising potential as TBC materials. Gd₂Zr₂O₇ and Y₂SiO₅, two recently developed thermal barrier coating (TBC) materials, have minimal thermal conductivities (K_{min}) of 1.22 W/m.K. and 1.3 W/m.K. [72], respectively, as confirmed by experiment. These numbers roughly match the values we computed for M₂AB₂ (M = Mo, Ta, and A = Ga, Ge).

The Grüneisen parameter (γ) is a crucial thermal parameter that helps explain the anharmonic effects of lattice dynamics; solids utilized at high temperatures are expected to have lower anharmonic effects. The Grüneisen parameter (γ) can be determined with the help of Poisson's ratio using equation (S16) [73]. The computed γ values, as shown in Table 6, suggest that the compounds under investigation exhibit a weak anharmonic effect. Additionally, for solids with a Poisson's ratio between 0.05 and 0.46, the values similarly fall within the range of 0.85 and 3.53 [74].

The melting temperature (T_m) of the compounds under investigation has been calculated using the following formula (S17). The strength of atomic bonding is the primary factor determining the melting temperature of solids; the higher the T_m , the stronger the atomic bonding. The order of T_m for the titled phases is found to mirror the Y -based (Young's modulus) order, indicating a close link between T_m and Y [75]. As observed in Table 6, our compounds roughly follow the Y -based ranking with $\text{Mo}_2\text{GeB}_2 < \text{Mo}_2\text{GaB}_2 < \text{Ta}_2\text{GeB}_2 < \text{Ta}_2\text{GaB}_2$. The T_m value for M_2AB_2 ($\text{M} = \text{Mo}, \text{Ta}$, and $\text{A} = \text{Ga}, \text{Ge}$) is also comparable with the TBC material $\text{Y}_4\text{Al}_2\text{O}_9$ (2000 K)[75].

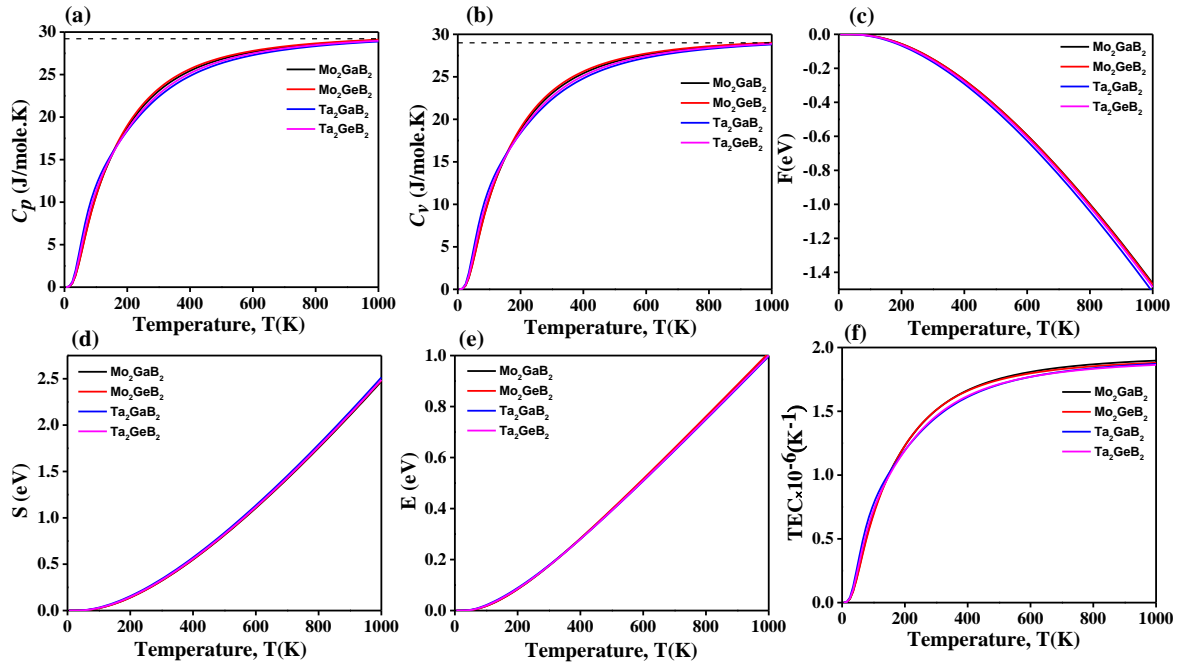


Fig. 6: Temperature dependence of the calculated thermodynamic parameters. (a) Specific heat at constant pressure, C_p (b) Specific heat at constant volume, C_v (c) Free energy, F (d) Entropy, S (e) Internal energy, E and (f) Thermal expansion coefficient, TEC of M_2AB_2 ($\text{M} = \text{Mo}, \text{Ta}$, and $\text{A} = \text{Ga}, \text{Ge}$).

The temperature dependence of specific heats, C_v , C_p , for the M_2AB_2 ($\text{M} = \text{Mo}, \text{Ta}$, and $\text{A} = \text{Ga}, \text{Ge}$) compounds was obtained using the formulas (S19-S20), as shown in Fig.6(a,b). Assuming that the quasi-harmonic model is accurate and that phase transitions are not anticipated for the compounds under study, these properties are approximated across a temperature range of 0 to 1000 K. Because phonon thermal softening occurs at higher temperatures, the heat capacity rises with temperature. Heat capacities increase quickly and follow the Debye- T^3 power law at lower

temperatures. At higher temperature regimes, where C_v and C_p do not greatly depend on temperature, they approach the Dulong-Petit ($3nN_Ak_B$) limit.[76].

Using the quasi-harmonic approximation, various temperature-dependent thermodynamic potential functions for M_2AB_2 ($M = \text{Mo, Ta, and } A = \text{Ga, Ge}$) have been estimated at zero pressure and displayed in Fig.6 [77]. These functions include the Helmholtz free energy (F), internal energy (E), and entropy (S) within 0-1000 K temperature using equation (S21-S23). The free energy progressively decreases as the temperature rises, as shown in Fig.6(c). Free energy typically declines, and this trend becomes increasingly negative as a natural process proceeds. As demonstrated in Fig. 6(d), the internal energy (E) shows a rising trend with temperature, in contrast to the free energy. Since thermal agitation creates disorder, a system's entropy rises as temperature rises. This is illustrated in Fig.6(d). A material's thermal expansion coefficient (TEC) is derived from the anharmonicity in the lattice dynamics and can be found using equation (S18). The measure of a material's capacity to expand or contract with heat or cold is called the Thermal Expansion Coefficient, or TEC. As observed in Fig. 5(f), the Thermal Expansion Coefficient (TEC) increases rapidly up to 365 K. Then it approaches a constant value, which indicates lower saturations in the materials with temperature changes. The materials under study have a very low TEC value, a crucial characteristic of materials intended for application in high-temperature technology.

To be effective as thermal barrier coating (TBC) materials, compounds must exhibit a low thermal conductivity (K_{\min}) to impede heat transfer, a high melting temperature to withstand extreme heat, and a low thermal expansion coefficient (TEC) to maintain dimensional stability under thermal stress. The compounds M_2AB_2 (where $M = \text{Mo, Ta, and } A = \text{Ga, Ge}$) possess these properties, making them suitable candidates for use as TBC materials

3.6 Optical Properties

Different materials exhibit unique behaviors when exposed to electromagnetic radiation. The optical constants determine the overall response of the sample to the incident radiation. The complex dielectric function, defined as $\varepsilon(\omega) = \varepsilon_1(\omega) + i\varepsilon_2(\omega)$, is one of the main optical characteristics of solids. The following formula determines the imaginary part of the dielectric function $\varepsilon_2(\omega)$ from the momentum matrix element between the occupied and unoccupied electronic states.

$$\varepsilon_2(\omega) = \frac{2e^2\pi}{\Omega\varepsilon_0} \sum_{k,v,c} |\psi_k^c| u \cdot r |\psi_k^v|^2 \delta(E_k^c - E_k^v - E)$$

In this formula, e stands for an electronic charge, ω for light angular frequency, u for the polarization vector of the incident electric field, and ψ_k^c and ψ_k^v for the conduction and valence band wave functions, respectively, at k . The Kramers-Kronig equation can estimate the real part of the dielectric function, $\varepsilon_1(\omega)$. In contrast, $\varepsilon_2(\omega)$ and $\varepsilon_1(\omega)$ are utilized to evaluate all other optical parameters, such as the absorption coefficient, photoconductivity, reflectivity, and loss function [78]. In this part, several energy-dependent optical properties of M_2AB_2 ($M = Mo, Ta$, and $A = Ga, Ge$) 212 MAX phases are calculated and analyzed in detail for the photon energy range of 0 to 30 eV, for [100] plane enabling the first assessment of the compounds' practical applicability.

Given the metallic conductivity of the MAX compounds' electronic structure, additional parameters were chosen to analyze the optical properties. These include a plasma frequency of 3 eV, damping of 0.05 eV, and Gaussian smearing of 0.5 eV [79].

Figure 7(a) shows the real component of the dielectric function, ε_1 , which exhibits metallic behavior. In metallic systems, ε_1 has a considerably high negative value in the low-energy range, with the real component reaching negative, which aligns with the band structure finding. Fig. 7(b) depicts the imaginary part of the dielectric function, $\varepsilon_2(\omega)$, representing dielectric losses about frequency. Mo_2GeB_2 demonstrates the highest peak in the low-energy region, with all compounds approaching zero from above at around 17 eV. This observation confirms Drude's behavior.

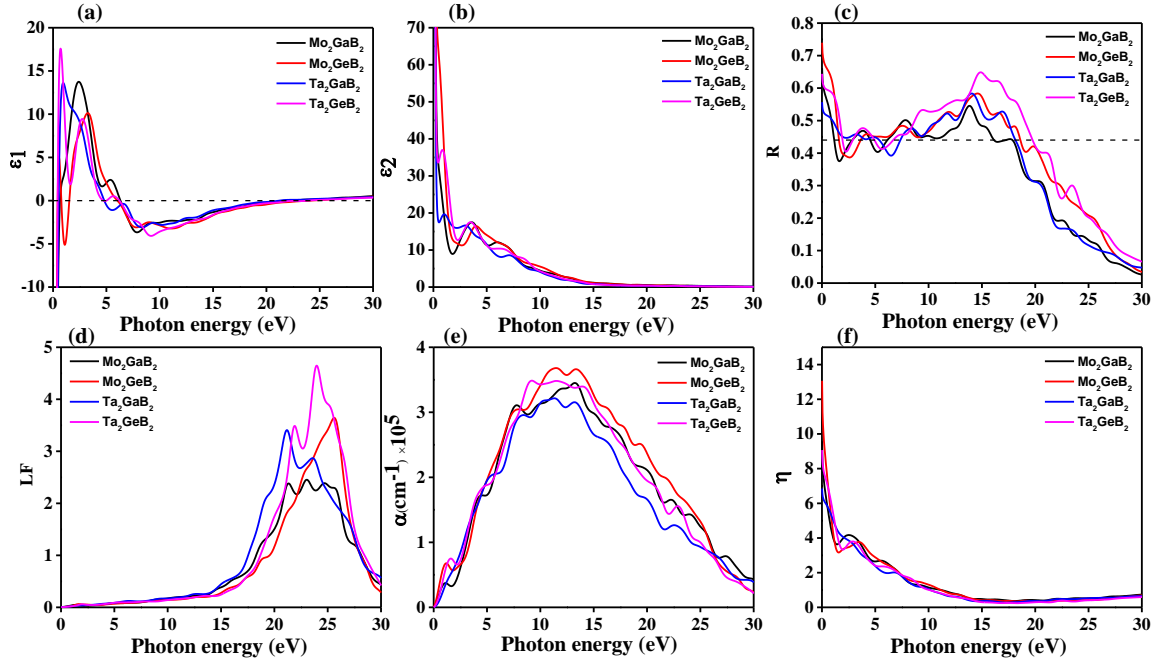


Fig. 7- (a) Real part of dielectric constant, ϵ_1 (b) Imaginary part of dielectric constant, ϵ_2 (c) Reflectivity, R and (d) Loss function, (e) The coefficient of absorption, (α) (f) Refractive index, (n) of M_2AB_2 ($M = Mo, Ta$, and $A = Ga, Ge$) for $[100]$ electric field directions.

The reflectivity of a material measures the percentage of incident light energy reflected off it. Equation (S24) was employed to compute reflectivity using the dielectric function, as shown in Fig.7(c). The spectra's visible and infrared (IR) portions consistently exhibit values exceeding 55%. Consequently, the materials under examination are expected to appear metallic gray. In the infrared (IR) region, the maximum reflectivity for Mo_2GaB_2 and Mo_2GeB_2 is 65% and 74%, respectively, occurring at 0.33 eV. Conversely, for Ta_2GaB_2 , the maximum reflectivity is 59% at 14.02 eV, while for Ta_2GeB_2 , it is 65% at 14.78 eV in the UV region. After 18 eV, the reflectance decreases significantly. According to reports, substances with an average reflectivity value above 44% in the visible light region can effectively reduce solar heating by reflecting a significant amount of the solar spectrum. Among all the compounds we examined, Ta_2GaB_2 has a reflectivity in the visible range of more than 44% [78]. Therefore, Ta_2GaB_2 can be utilized as a coating material and should be able to mitigate solar heating.

Equation (S25) yielded the energy loss function, $LF(\omega)$ spectra of the compounds M_2AB_2 ($M = Mo, Ta$, and $A = Ga, Ge$), which are displayed in Fig.7(d) with the peaks corresponding to

plasma frequencies (ω_p). The plasma frequency for Mo_2GaB_2 , Mo_2GeB_2 , Ta_2GaB_2 , and Ta_2GeB_2 is observed at 23 eV, 25 eV, 21 eV, and 23 eV, respectively. At this specific frequency, the absorption coefficient rapidly decreases, ε_1 crosses zero from the negative side, and the reflectance $R(\omega)$ displays a falling tail. Above this distinctive frequency, the materials are transparent to the incident electromagnetic radiation.

Fig. 7(e) illustrates the absorbance coefficient (α) of compounds M_2AB_2 ($\text{M} = \text{Mo}, \text{Ta}$, and $\text{A} = \text{Ga}, \text{Ge}$) determined using equation (S26). As α begins to rise from zero photon energy, the metallic nature of the substances under study is again indicated. The visible light region experiences a sharp increase in absorption, peaking in the UV region at around 14 eV and then progressively declining. The IR region exhibits negligible absorption. However, the materials mentioned above appear to have a significant absorption band primarily located in the visible and ultraviolet spectrum. This suggests that the materials can be used in UV surface-disinfection devices, medical sterilization equipment, and other optoelectronic device designs.

Its refractive index is crucial to a material's potential application in optical devices like waveguides and photonic crystals. Equations (S27) and (S28) were used to derive the refractive index (n) and extinction coefficient (k) for M_2AB_2 ($\text{M} = \text{Mo}, \text{Ta}$, and $\text{A} = \text{Ga}, \text{Ge}$), as depicted in Fig.7(c) and Fig.S-1(a). The variations of n and k in MAX phase carbides with incident photon energy closely resemble $\varepsilon_1(\omega)$ and $\varepsilon_2(\omega)$. The static refractive index $n(0)$ for Mo_2GaB_2 , Mo_2GeB_2 , Ta_2GaB_2 , and Ta_2GeB_2 is 9.4, 13.07, 7 and 9.2, respectively, and decreases gradually with the increase in photon energy. The extinction coefficient for Mo_2GaB_2 , Mo_2GeB_2 , Ta_2GaB_2 , and Ta_2GeB_2 gradually increases in the IR region, reaching their maximum values of 2.56, 4.27, 2.42, and 3.28, respectively. Following this, they slowly decrease in the visible and UV regions.

Figure S-1(b) illustrates the photoconductivity (σ) of M_2AB_2 ($\text{M} = \text{Mo}, \text{Ta}$, and $\text{A} = \text{Ga}, \text{Ge}$) across various photon energies. The photoconductivity (σ) parameter quantifies the impact of photon irradiation on a material's electrical conductivity. Similar to the absorbance coefficient (α) spectrum, the σ spectrum aligns with the metallic nature of M_2AB_2 ($\text{M} = \text{Mo}, \text{Ta}$, and $\text{A} = \text{Ga}, \text{Ge}$).

4 Conclusions

In summary, we employed DFT calculations to explore four 212 MAB phases, M_2AB_2 ($M = Mo, Ta$, and $A = Ga, Ge$), and investigated the structural, electronic, mechanical, lattice dynamical, and optical properties to predict their possible applications. The phonon dispersion curves, formation energy, and elastic constants collectively suggest that the M_2AB_2 boride maintains dynamic, mechanical, chemical, and thermodynamic stability. The electronic band structure and density of states (DOS) offer evidence supporting the metallic nature of the compounds under investigation. Concurrently, the charge density mapping and atomic Mulliken population both confirm the presence of a strong B-B covalent bond. The stiffness constants, elastic moduli, f -index, fracture toughness (K_{IC}), Pugh's ratio (G/B), hardness parameters, and Cauchy Pressure (CP) of M_2AB_2 were computed and compared with those of their 211 equivalents. We found that the values of the 212-phase borides are higher than those of the 211-phase carbides or borides. Mo_2GaB_2 and Ta_2GaB_2 are identified as brittle solids, while Mo_2GeB_2 and Ta_2GeB_2 exhibit ductile characteristics, as indicated by Poisson's ratio (ν) and Pugh's ratio (B/G or G/B). The elastic characteristics display anisotropy due to the distinct atomic configurations along the a - and c -directions. Vickers hardness calculations are considered reliable indicators of material hardness. The results suggest that Mo_2GaB_2 and Mo_2GeB_2 possess more pliable characteristics than Ta_2GaB_2 and Ta_2GeB_2 . The high hardness values of Ta_2GaB_2 and Ta_2GeB_2 compared to the Mo_2GaB_2 and Mo_2GeB_2 due to higher BOP values of M-B bonding in Ta_2GaB_2 and Ta_2GeB_2 than in Mo_2GaB_2 and Mo_2GeB_2 . The value of minimum thermal conductivity (K_{min}), thermal expansion coefficient, and melting temperature (T_m) collectively suggest the potential suitability of M_2AB_2 ($M = Mo, Ta$, and $A = Ga, Ge$) as a material for thermal barrier coating (TBC) applications in high-temperature devices. The optical conductivity and absorption coefficient corroborate the findings of the electronic band structure. Reflectivity is notably high in infrared (IR) regions and remains nearly constant in the visible and moderate ultraviolet (UV) regions, with an average value exceeding 44% for Ta_2GaB_2 . This suggests that Ta_2GaB_2 can be effectively utilized as a coating material to reduce solar heating. We expect that the comprehensive analysis of the diverse physical characteristics of M_2AB_2 ($M = Mo, Ta$, and $A = Ga, Ge$) presented in this study will establish a robust foundation for future theoretical and experimental explorations of these fascinating MAB phases.

CRediT author statement

A. K. M Naim Ishtiaq and Md Nasir Uddin: Data curation, Writing- Original draft preparation. Md. Rasel Rana, Shariful Islam and Noor Afsary: Reviewing and Editing. Md. Ashraf Ali: Methodology, Reviewing and Editing, conceptualization, supervision; and Karimul Hoque: conceptualization, supervision, editing, and reviewing.

Declaration of interests

The authors declare that they have no known competing financial interests or personal relationships that could have appeared to influence the work reported in this paper.

Acknowledgments

The authors acknowledge Physics Discipline, Khulna University, Khulna for the logistic support and Advanced Computational Materials Research Laboratory (ACMRL), Department of Physics at Chittagong University of Engineering & Technology (CUET), Chattogram-4349, Bangladesh for laboratory facilities.

- [1] M. W. Barsoum, G. Yaroschuk, and S. Tyagi, “Fabrication and characterization of M_2SnC ($M = Ti, Zr, Hf$ and Nb),” *Scr. Mater.*, vol. 37, no. 10, pp. 1583–1591, 1997, doi: 10.1016/S1359-6462(97)00288-1.
- [2] M. W. Barsoum and T. El-Raghy, “Synthesis and characterization of a remarkable ceramic: Ti_3SiC_2 ,” *Journal of the American Ceramic Society*, vol. 79, no. 7. pp. 1953–1956, 1996. doi: 10.1111/j.1151-2916.1996.tb08018.x.
- [3] M. A. Ali, M. M. Hossain, M. M. Uddin, A. K. M. A. Islam, and S. H. Naqib, “Enhanced thermo-mechanical properties of 212 MAX phase borides Zr_2AB_2 ($A = In, Ti$): an ab-initio understanding,” vol. 2.
- [4] M. Radovic and M. W. Barsoum, “MAX phases: Bridging the gap between metals and ceramics,” *Am. Ceram. Soc. Bull.*, vol. 92, no. 3, pp. 20–27, 2013.
- [5] M. W. Barsoum and M. Radovic, “Elastic and mechanical properties of the MAX phases,” *Annu. Rev. Mater. Res.*, vol. 41, pp. 195–227, 2011, doi: 10.1146/annurev-matsci-062910-100448.

- [6] J. L. Smialek and S. Gray, "Type II Hot Corrosion Screening Tests of a Cr₂AlC MAX Phase Compound," *Oxid. Met.*, vol. 90, no. 5–6, pp. 555–570, 2018, doi: 10.1007/s11085-018-9857-2.
- [7] J. Sarwar, T. Shrouf, A. Srinivasa, H. Gao, M. Radovic, and K. Kakosimos, "Characterization of thermal performance, flux transmission performance and optical properties of MAX phase materials under concentrated solar irradiation," *Sol. Energy Mater. Sol. Cells*, vol. 182, no. March, pp. 76–91, 2018, doi: 10.1016/j.solmat.2018.03.018.
- [8] M. Naguib *et al.*, "Two-dimensional nanocrystals produced by exfoliation of Ti₃AlC₂," *Adv. Mater.*, vol. 23, no. 37, pp. 4248–4253, 2011, doi: 10.1002/adma.201102306.
- [9] T. Lapauw *et al.*, "Interaction of Mn₂AlX_n phases with oxygen-poor, static and fast-flowing liquid lead-bismuth eutectic," *J. Nucl. Mater.*, vol. 520, pp. 258–272, 2019, doi: 10.1016/j.jnucmat.2019.04.010.
- [10] T. Rackl, L. Eisenburger, R. Niklaus, and D. Johrendt, "Syntheses and physical properties of the MAX phase boride Nb₂SB and the solid solutions Nb₂S_{1-x}B_x C_{1-x}(x=0–1)," *Phys. Rev. Mater.*, vol. 3, no. 5, pp. 1–7, 2019, doi: 10.1103/PhysRevMaterials.3.054001.
- [11] O. O. Kurakevych, "Superhard phases of simple substances and binary compounds of the B-C-N-O system: From diamond to the latest results (a Review)," *J. Superhard Mater.*, vol. 31, no. 3, pp. 139–157, 2009, doi: 10.3103/S1063457609030010.
- [12] M. Sheikholeslami, D. D. Ganji, and I. Nuclear, "50 + years of INIS," *Chem. Phys. Lett.*, vol. 7, no. 17001963, pp. 164–165, 2017, [Online]. Available: <http://dx.doi.org/10.1016/j.cplett.2016.11.013>
- [13] M. Ade and H. Hillebrecht, "Ternary Borides Cr₂AlB₂, Cr₃AlB₄, and Cr₄AlB₆: The First Members of the Series (CrB₂)_nCrAl with n = 1, 2, 3 and a Unifying Concept for Ternary Borides as MAB-Phases," *Inorg. Chem.*, vol. 54, no. 13, pp. 6122–6135, 2015, doi: 10.1021/acs.inorgchem.5b00049.
- [14] H. Zhang, F. zhi Dai, H. Xiang, Z. Zhang, and Y. Zhou, "Crystal structure of Cr₄AlB₄: A new MAB phase compound discovered in Cr-Al-B system," *J. Mater. Sci. Technol.*, vol.

- 35, no. 4, pp. 530–534, 2019, doi: 10.1016/j.jmst.2018.10.006.
- [15] M. Khazaei, M. Arai, T. Sasaki, M. Estili, and Y. Sakka, “Trends in electronic structures and structural properties of MAX phases: A first-principles study on M_2AlC ($M = Sc, Ti, Cr, Zr, Nb, Mo, Hf$, or Ta), M_2AlN , and hypothetical M_2AlB phases,” *J. Phys. Condens. Matter*, vol. 26, no. 50, 2014, doi: 10.1088/0953-8984/26/50/505503.
- [16] S. Islam *et al.*, “A comprehensive exploration of the physical properties of M_2GaB ($M = Ti, Zr, Mo, Hf$) through DFT method,” *Results Mater.*, vol. 19, no. July, p. 100438, 2023, doi: 10.1016/j.rinma.2023.100438.
- [17] A. K. M. N. Ishtiaq *et al.*, “First-principles study of electronic, mechanical, and optical properties of M_3GaB_2 ($M = Ti, Hf$) MAX phases,” *Heliyon*, vol. 10, no. 13, p. e33651, 2024, doi: 10.1016/j.heliyon.2024.e33651.
- [18] L. Chen *et al.*, “Theoretical Prediction and Synthesis of $(Cr_{2/3}Zr_{1/3})_2AlC$ i-MAX Phase,” *Inorg. Chem.*, vol. 57, no. 11, pp. 6237–6244, 2018, doi: 10.1021/acs.inorgchem.8b00021.
- [19] M. W. Qureshi, M. A. Ali, and X. Ma, “Screen the thermomechanical and optical properties of the new ductile 314 MAX phase boride Zr_3CdB_4 : A DFT insight,” *J. Alloys Compd.*, vol. 877, p. 160248, 2021, doi: 10.1016/j.jallcom.2021.160248.
- [20] Y. Liu, Z. Jiang, X. Jiang, and J. Zhao, “New refractory MAB phases and their 2D derivatives: Insight into the effects of valence electron concentration and chemical composition,” *RSC Adv.*, vol. 10, no. 43, pp. 25836–25847, 2020, doi: 10.1039/d0ra04385k.
- [21] M. A. Ali, M. M. Hossain, A. K. M. A. Islam, and S. H. Naqib, “Ternary boride Hf_3PB_4 : Insights into the physical properties of the hardest possible boride MAX phase,” *J. Alloys Compd.*, vol. 857, p. 158264, 2021, doi: 10.1016/j.jallcom.2020.158264.
- [22] Y. X. Wang, Z. X. Yan, W. Liu, and G. L. Zhou, “Structure stability, mechanical properties and thermal conductivity of the new hexagonal ternary phase Ti_2InB_2 under pressure,” *Philos. Mag.*, vol. 100, no. 16, pp. 2054–2067, 2020, doi: 10.1080/14786435.2020.1754485.
- [23] N. Miao *et al.*, “Computational prediction of boron-based MAX phases and MXene

- derivatives,” *Chem. Mater.*, vol. 32, no. 16, pp. 6947–6957, 2020, doi: 10.1021/acs.chemmater.0c02139.
- [24] J. Wang *et al.*, “Discovery of hexagonal ternary phase Ti_2InB_2 and its evolution to layered boride TiB ,” *Nat. Commun.*, vol. 10, no. 1, pp. 1–8, 2019, doi: 10.1038/s41467-019-10297-8.
- [25] M. A. Ali, M. M. Hossain, M. M. Uddin, A. K. M. A. Islam, and S. H. Naqib, “Understanding the improvement of thermo-mechanical and optical properties of 212 MAX phase borides Zr_2AB_2 ($A = \text{In, Tl}$),” *J. Mater. Res. Technol.*, vol. 15, pp. 2227–2241, 2021, doi: 10.1016/j.jmrt.2021.09.042.
- [26] M. A. Ali, M. M. Hossain, M. M. Uddin, A. K. M. A. Islam, D. Jana, and S. H. Naqib, “DFT insights into new B-containing 212 MAX phases: Hf_2AB_2 ($A = \text{In, Sn}$),” *J. Alloys Compd.*, vol. 860, 2021, doi: 10.1016/j.jallcom.2020.158408.
- [27] G. Surucu, “Investigation of structural, electronic, anisotropic elastic, and lattice dynamical properties of MAX phases borides: An Ab-initio study on hypothetical M_2AB ($M = \text{Ti, Zr, Hf}$; $A = \text{Al, Ga, In}$) compounds,” *Mater. Chem. Phys.*, vol. 203, pp. 106–117, 2018, doi: 10.1016/j.matchemphys.2017.09.050.
- [28] A. S. Ingason *et al.*, “A nanolaminated magnetic phase: Mn_2GaC ,” *Mater. Res. Lett.*, vol. 2, no. 2, pp. 89–93, 2014, doi: 10.1080/21663831.2013.865105.
- [29] S. J. Clark *et al.*, “First principles methods using CASTEP,” *Zeitschrift fur Krist.*, vol. 220, no. 5–6, pp. 567–570, 2005, doi: 10.1524/zkri.220.5.567.65075.
- [30] M. D. Segall *et al.*, “First-principles simulation: Ideas, illustrations and the CASTEP code,” *J. Phys. Condens. Matter*, vol. 14, no. 11, pp. 2717–2744, 2002, doi: 10.1088/0953-8984/14/11/301.
- [31] J. P. Perdew, K. Burke, and M. Ernzerhof, “Generalized gradient approximation made simple,” *Phys. Rev. Lett.*, vol. 77, no. 18, pp. 3865–3868, 1996, doi: 10.1103/PhysRevLett.77.3865.
- [32] T. H. Fischer and J. Almlöf, “General methods for geometry and wave function optimization,” *J. Phys. Chem.*, vol. 96, no. 24, pp. 9768–9774, 1992, doi:

10.1021/j100203a036.

- [33] D. Roundy and M. L. Cohen, “Ideal strength of diamond, Si, and Ge,” *Phys. Rev. B - Condens. Matter Mater. Phys.*, vol. 64, no. 21, pp. 2–4, 2001, doi: 10.1103/PhysRevB.64.212103.
- [34] M. A. Ali, M. M. Hossain, M. M. Uddin, A. K. M. A. Islam, and S. H. Naqib, “The Rise of 212 MAX Phase Borides: DFT Insights into the Physical Properties of Ti_2PB_2 , Zr_2PbB_2 , and Nb_2AB_2 [$A = P, S$] for Thermomechanical Applications,” *ACS Omega*, vol. 8, no. 1, pp. 954–968, 2023, doi: 10.1021/acsomega.2c06331.
- [35] M. R. Rana *et al.*, “DFT prediction of the stability and physical properties of M_2GaB ($M = Sc, V, Nb, Ta$),” *J. Mater. Res. Technol.*, vol. 24, pp. 7795–7815, 2023, doi: 10.1016/j.jmrt.2023.05.008.
- [36] M. Zr *et al.*, “Structural Stability, Electronic, Mechanical, Phonon, and Thermodynamic Properties of the M_2GaC ($M = Zr, Hf$) MAX Phase: An ab Initio Calculation,” 2020.
- [37] R. Steinitz, I. Binder, and D. Moskowitz, “System Molybdenum-Boron and Some Properties of The Molybdenum-Borides,” *Jom*, vol. 4, no. 9, pp. 983–987, 1952, doi: 10.1007/bf03397758.
- [38] E. Rudy, F. Benesovsky, and L. Toth, “No Title,” *Int. J. Mater. Res.*, vol. 54, no. 6, pp. 345–353, 1963, doi: doi:10.1515/ijmr-1963-540604.
- [39] S. Kirklin *et al.*, “The Open Quantum Materials Database (OQMD): Assessing the accuracy of DFT formation energies,” *npj Comput. Mater.*, vol. 1, no. September, 2015, doi: 10.1038/npjcompumats.2015.10.
- [40] I. Higashi, Y. Takahashi, and S. Okada, “Crystal structure of MoB_2 ,” *J. Less-Common Met.*, vol. 123, no. 1–2, pp. 277–283, 1986, doi: 10.1016/0022-5088(86)90136-0.
- [41] W. Zulfiqar, S. M. Alay-E-Abbas, G. Abbas, A. Laref, J. A. Larsson, and A. Shaukat, “Revisiting the structural, electronic and photocatalytic properties of Ti and Zr based perovskites with meta-GGA functionals of DFT,” *J. Mater. Chem. C*, vol. 9, no. 14, pp. 4862–4876, 2021, doi: 10.1039/d0tc05964a.

- [42] K. Refson, P. R. Tulip, and S. J. Clark, “Variational density-functional perturbation theory for dielectrics and lattice dynamics,” *Phys. Rev. B - Condens. Matter Mater. Phys.*, vol. 73, no. 15, pp. 1–12, 2006, doi: 10.1103/PhysRevB.73.155114.
- [43] F. Mouhat and F. X. Coudert, “Necessary and sufficient elastic stability conditions in various crystal systems,” *Phys. Rev. B - Condens. Matter Mater. Phys.*, vol. 90, no. 22, pp. 4–7, 2014, doi: 10.1103/PhysRevB.90.224104.
- [44] Y. Zhou and Z. Sun, “Electronic structure and bonding properties of layered machinable and ceramics,” *Phys. Rev. B - Condens. Matter Mater. Phys.*, vol. 61, no. 19, pp. 12570–12573, 2000, doi: 10.1103/PhysRevB.61.12570.
- [45] M. N. Uddin, A. K. M. N. Ishtiaq, S. Islam, M. R. Rana, M. A. Ali, and K. Hoque, “Prediction of new 212 M₂AB₂ borides as a promising candidate for future engineering: DFT calculations,” *Mater. Today Commun.*, p. 108536, 2024, doi: <https://doi.org/10.1016/j.mtcomm.2024.108536>.
- [46] F. Ernst and M. Ruhle, Eds., *High-resolution imaging and spectrometry of materials*. in Springer series in materials science. Berlin, Germany: Springer, 2010.
- [47] M. A. Ali, A. K. M. A. Islam, N. Jahan, and S. Karimunnesa, “First-principles study of SnO under high pressure,” *Int. J. Mod. Phys. B*, vol. 30, no. 31, pp. 1–12, 2016, doi: 10.1142/S0217979216502283.
- [48] M. A. Ali and A. K. M. A. Islam, “Sn 1-xBi xO 2 and Sn 1-xTa xO 2 (0≤x≤0.75): A first-principles study,” *Phys. B Condens. Matter*, vol. 407, no. 6, pp. 1020–1026, 2012, doi: 10.1016/j.physb.2012.01.002.
- [49] L. Fast, J. M. Wills, B. Johansson, and O. Eriksson, “Elastic constants of hexagonal transition metals: Theory,” *Phys. Rev. B*, vol. 51, no. 24, pp. 17431–17438, 1995, doi: 10.1103/PhysRevB.51.17431.
- [50] M. M. Ali, M. A. Hadi, I. Ahmed, A. F. M. Y. Haider, and A. K. M. A. Islam, “Physical properties of a novel boron-based ternary compound Ti₂InB₂,” *Mater. Today Commun.*, vol. 25, no. June, p. 101600, 2020, doi: 10.1016/j.mtcomm.2020.101600.
- [51] D. G. Pettifor, “Theoretical predictions of structure and related properties of

- intermetallics,” *Mater. Sci. Technol. (United Kingdom)*, vol. 8, no. 4, pp. 345–349, 1992, doi: 10.1179/mst.1992.8.4.345.
- [52] M. A. Ali, M. M. Hossain, M. M. Uddin, A. K. M. A. Islam, and S. Naqib, “The Rise of 212 Max Phase Borides, Ti_2pb_2 , Zr_2pbb_2 , and Nb_2ab_2 [A = P, S]: Dft Insights into the Physical Properties for Thermo-Mechanical Applications,” *SSRN Electron. J.*, 2022, doi: 10.2139/ssrn.4225641.
- [53] I. R. Shein and A. L. Ivanovskii, “Elastic properties of superconducting MAX phases from first-principles calculations,” *Phys. Status Solidi Basic Res.*, vol. 248, no. 1, pp. 228–232, 2011, doi: 10.1002/pssb.201046163.
- [54] B. R. Hill H H, “138,330 ; 1932 B,” *Dokl., Akad. Nauk. SSSR*, vol. 129, p. 484, 1932.
- [55] W. Voigt, *Lehrbuch der kristallphysik:(mit ausschluss der kristalloptik)*, vol. 34. BG Teubner, 1910.
- [56] A. Reuss, “Berechnung der Fließgrenze von Mischkristallen auf Grund der Plastizitätsbedingung für Einkristalle .,” *ZAMM - J. Appl. Math. Mech. / Zeitschrift für Angew. Math. und Mech.*, vol. 9, no. 1, pp. 49–58, 1929, doi: 10.1002/zamm.19290090104.
- [57] M. F. Cover, O. Warschkow, M. M. M. Bilek, and D. R. McKenzie, “A comprehensive survey of M2AX phase elastic properties,” *J. Phys. Condens. Matter*, vol. 21, no. 30, 2009, doi: 10.1088/0953-8984/21/30/305403.
- [58] Z. M. Sun, “Progress in research and development on MAX phases: a family of layered ternary compounds,” *Int. Mater. Rev.*, vol. 56, no. 3, pp. 143–166, May 2011, doi: 10.1179/1743280410Y.0000000001.
- [59] S. Aryal, R. Sakidja, M. W. Barsoum, and W. Y. Ching, “A genomic approach to the stability, elastic, and electronic properties of the MAX phases,” *Phys. Status Solidi Basic Res.*, vol. 251, no. 8, pp. 1480–1497, 2014, doi: 10.1002/pssb.201451226.
- [60] I. N. Frantsevich, F. F. Voronov, and S. A. Bokuta, “Elastic Constants and Elastic Moduli of Metals and Insulators Handbook,” 1983.

- [61] P. Das, N. Jahan, and M. A. Ali, "DFT insights into Nb-based 211 MAX phase carbides: Nb₂AC (A = Ga, Ge, Tl, Zn, P, In, and Cd)," *RSC Adv.*, vol. 13, no. 8, pp. 5538–5556, 2023, doi: 10.1039/D2RA07468K.
- [62] H. M. Ledbetter, "Elastic properties of zinc: A compilation and a review," *J. Phys. Chem. Ref. Data*, vol. 6, no. 4, pp. 1181–1203, 1977, doi: 10.1063/1.555564.
- [63] S. I. Ranganathan and M. Ostoja-Starzewski, "Universal elastic anisotropy index," *Phys. Rev. Lett.*, vol. 101, no. 5, pp. 3–6, 2008, doi: 10.1103/PhysRevLett.101.055504.
- [64] H. Figiel, O. Zogał, and V. Yartys, "Journal of Alloys and Compounds: Preface," *J. Alloys Compd.*, vol. 404–406, no. SPEC. ISS., p. 1, 2005, doi: 10.1016/j.jallcom.2005.05.002.
- [65] A. Ali, M. Hossain, M. Uddin, A. K. M. A. Islam, and S. H. Naqib, "The Rise of 212 MAX Phase Borides : DFT Insights into the Physical Thermomechanical Applications," 2023, doi: 10.1021/acsomega.2c06331.
- [66] H. Gou, L. Hou, J. Zhang, and F. Gao, "Pressure-induced incompressibility of ReC and effect of metallic bonding on its hardness," *Appl. Phys. Lett.*, vol. 92, no. 24, pp. 0–3, 2008, doi: 10.1063/1.2938031.
- [67] M. N. Uddin, A. K. M. N. Ishtiaq, S. Islam, M. R. Rana, M. A. Ali, and K. Hoque, "Prediction of new 212 M₂AB₂ borides as a promising candidate for future engineering: DFT calculations," *Mater. Today Commun.*, vol. 39, no. June, p. 108536, 2024, doi: 10.1016/j.mtcomm.2024.108536.
- [68] O. L. Anderson, "a Simplified Method for Calculating the," *J. Phys. Chem. Solids*, vol. 24, pp. 909–917, 1963.
- [69] M. A. Hadi, M. Dahlqvist, S. R. G. Christopoulos, S. H. Naqib, A. Chroneos, and A. K. M. A. Islam, "Chemically stable new MAX phase V₂SnC: A damage and radiation tolerant TBC material," *RSC Adv.*, vol. 10, no. 71, pp. 43783–43798, 2020, doi: 10.1039/d0ra07730e.
- [70] D. R. Clarke, "Materials selections guidelines for low thermal conductivity thermal barrier coatings," *Surf. Coatings Technol.*, vol. 163–164, pp. 67–74, 2003, doi: 10.1016/S0257-8972(02)00593-5.

- [71] Y. Liu *et al.*, “Discovery of ABO₃ perovskites as thermal barrier coatings through high-throughput first principles calculations,” *Mater. Res. Lett.*, vol. 7, no. 4, pp. 145–151, 2019, doi: 10.1080/21663831.2019.1566183.
- [72] B. Liu *et al.*, “Advances on strategies for searching for next generation thermal barrier coating materials,” *J. Mater. Sci. Technol.*, vol. 35, no. 5, pp. 833–851, 2019, doi: 10.1016/j.jmst.2018.11.016.
- [73] V. N. Belomestnykh and E. P. Tesleva, “Interrelation between anharmonicity and lateral strain in quasi-isotropic polycrystalline solids,” *Tech. Phys.*, vol. 49, no. 8, pp. 1098–1100, 2004, doi: 10.1134/1.1787679.
- [74] W. Other, O. F. Poissonvs, and O. F. Pure, “C-05-1,” *CESBP Cent. Eur. Symp. Build. Phys. / BauSIM 2016.*, vol. 18, no. 3, pp. 277–284, 2016, doi: 10.51202/9783816797982-277.
- [75] Y. Zhou, H. Xiang, X. Lu, Z. Feng, and Z. Li, “Theoretical prediction on mechanical and thermal properties of a promising thermal barrier material: Y₄Al₂O₉,” *J. Adv. Ceram.*, vol. 4, no. 2, pp. 83–93, 2015, doi: 10.1007/s40145-015-0140-6.
- [76] P. Debye, “Zur Theorie der spezifischen Wärmen,” *Ann. Phys.*, vol. 344, no. 14, pp. 789–839, 1912, doi: 10.1002/andp.19123441404.
- [77] F. Karsch, A. Patkós, and P. Petreczky, “Screened perturbation theory,” *Phys. Lett. Sect. B Nucl. Elem. Part. High-Energy Phys.*, vol. 401, no. 1–2, pp. 69–73, 1997, doi: 10.1016/S0370-2693(97)00392-4.
- [78] S. Li, R. Ahuja, M. W. Barsoum, P. Jena, and B. Johansson, “Optical properties of Ti₃SiC₂ and Ti₄AlN₃,” *Appl. Phys. Lett.*, vol. 92, no. 22, pp. 90–93, 2008, doi: 10.1063/1.2938862.
- [79] R. John and B. Merlin, “Optical properties of graphene, silicene, germanene, and stanene from IR to far UV – A first principles study,” *J. Phys. Chem. Solids*, vol. 110, pp. 307–315, 2017, doi: 10.1016/j.jpcs.2017.06.026.